CARBON-SUBLIMATION PRODUCTION OF FULLERENES

by

Frank Albert Tinker

A Dissertation Submitted to the Faculty of the

DEPARTMENT OF PHYSICS

In Partial Fulfillment of the Requirements
For the Degree of

DOCTOR OF PHILOSOPHY

In the Graduate College

THE UNIVERSITY OF ARIZONA

1 9 9 5

CARBON-SUBLIMATION PRODUCTION OF FULLERENES

by

Frank Albert Tinker

A Dissertation Submitted to the Faculty of the

DEPARTMENT OF PHYSICS

In Partial Fulfillment of the Requirements
For the Degree of

DOCTOR OF PHILOSOPHY

In the Graduate College

THE UNIVERSITY OF ARIZONA

1 9 9 5

THE UNIVERSITY OF ARIZONA
GRADUATE COLLEGE

As members of the Final Examination Committee, we certify that we have read the dissertation prepared by Frank Albert Tinker

entitled Carbon Sublimation Production of Fullerenes

and recommend that it be accepted as fulfilling the dissertation requirement for the Degree of Doctor of Philosophy

David Lott	5/9/95 Date
M. A. Shupe	5/9/95 Date
William S. Barnes	5/9/95 Date
Roy M. Emrick	9 May 95 Date
Donald R. Huffman	9 May 95 Date

Final approval and acceptance of this dissertation is contingent upon the candidate's submission of the final copy of the dissertation to the Graduate College.

I hereby certify that I have read this dissertation prepared under my direction and recommend that it be accepted as fulfilling the dissertation requirement.

Donald R. Huffman	5/29/95
Dissertation Director	Date

STATEMENT BY AUTHOR

This dissertation has been submitted in partial fulfillment of requirements for an advanced degree at The University of Arizona and is deposited in the University Library to be made available to borrowers under rules of the library.

Brief quotations from this dissertation are allowable without special permission, provided that accurate acknowledgment of source is made. Requests for permission for extended quotation from or reproduction of this manuscript in whole or in part may be granted by the head of the major department or the Dean of the Graduate College when in his or her judgment the proposed use of the material is in the interests of scholarship. In all other instances, however, permission must be obtained from the author.

SIGNED: 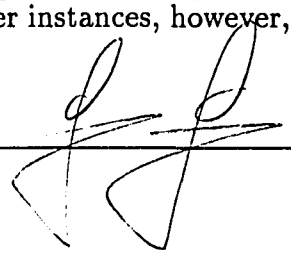

ACKNOWLEDGEMENTS

Professor Donald R. Huffman has provided reliable counsel, friendly encouragement, and leadership by example throughout my graduate career. For these, I am very grateful.

I also wish to thank Dr. Lowell D. Lamb, who has been generous with his time and suggestions.

For their encouragement, I thank my parents, Frank A. and Nancy Lee Tinker.

Finally, and most of all, I thank my wife, Janet. Her support, inspiration, and disposition made this journey possible.

TABLE OF CONTENTS

LIST OF FIGURES

ABSTRACT

Carbon-sublimation production of fullerenes enjoys wide use in both experimental and industrial application worldwide. Although it has been nearly five years since the inception of the technique, little is known about the roles various parameters play in the production process. This work attempts to shed light, both experimentally and theoretically, on the basic processes at work in this type of fullerene production.

Experimental results herein show that a functional relationship exists among the C_{60}, C_{70}, C_{76}, C_{78}, and C_{84} fullerenes produced in carbon arcs. This result is interpreted to mean that an equilibrium description of the production process may be valid. Theoretical calculations are then offered in support of such a view. The theory goes on to show details of an equilibrium description that reproduce essential features of fullerene mass-spectra.

It is shown that equilibrium abundances of n-atom-sized clusters are highly dependent on the stoichiometric equation chosen to describe the system. However, common traits of the investigated equilibrium descriptions lead to useful conclusions.

CHAPTER 1

INTRODUCTION

A 1984 paper [1] by an Exxon research group described an experiment where a high-pressure pulse of helium was introduced into an evacuated chamber and directed across the surface of a spinning graphite disk. A laser, timed to coincide with the arrival of the helium pulse, would then be fired at the graphite disk to create a cloud of carbon gas in the presence of the helium. The carbon/helium gas would continue across the spinning disk, through a short channel, and into a time-of-flight mass spectrometer (TOF-MS) where the carbon clusters were ionized and their sizes analyzed. The results of these experiments (see Fig. 1.1) revealed two, apparently disparate, carbon-cluster distributions. The low-mass family, C_n with $n < 30$, contained both odd and even numbers of atoms and were, therefore, spaced by C_1. The high-mass family, C_n with $n > 30$, were restricted to even numbers of atoms and C_2 spacing.

Further experiments by Kroto et al. [2] adjusted the laser timing to alter the ambient pressure at the evaporation point. Results from this study (see Fig. 1.2) revealed the anomalous stability of the C_{60} and C_{70} carbon clusters with respect to their neighbors. The group proposed that the structure of the highly stable C_{60} cluster was that of a truncated icosahedron (see figure 1.3). The geodesic character of the proposed structure prompted the name "buckminsterfullerene" or, more affectionately, "bucky ball", in honor of Buckminster Fuller, who devoted considerable effort to the study of geodesic structures.

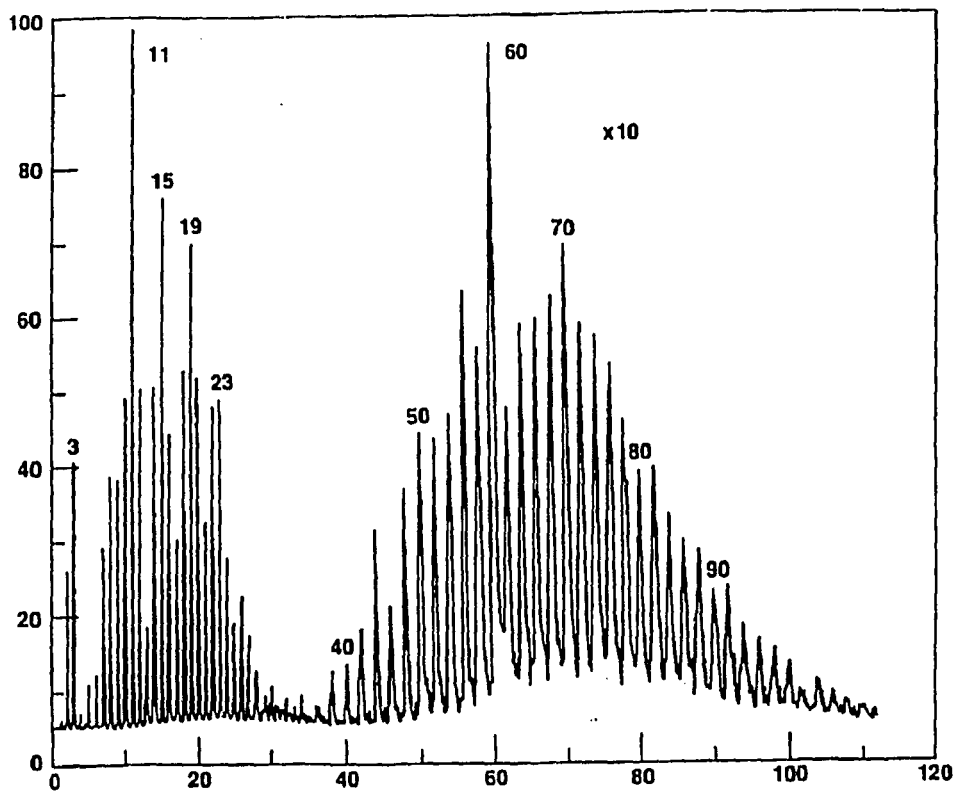

Figure 1.1: Carbon Cluster Mass Spectra as seen by the Exxon group [1] (used with permission from *Journal of Chemical Physics*).

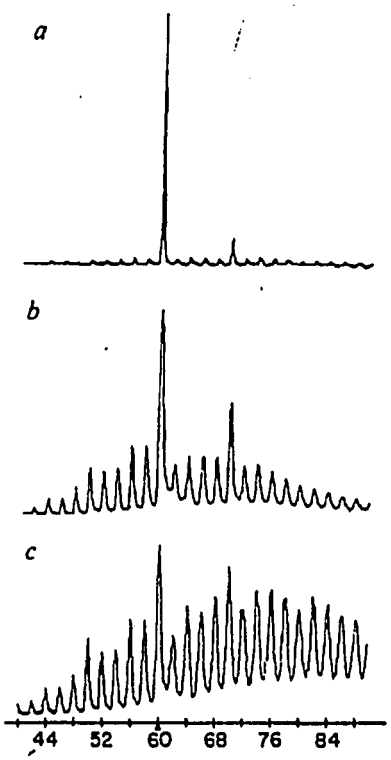

Figure 1.2: Carbon Cluster Mass Spectra as seen by Kroto et al. [2] showing cluster-abundance dependence on He pressure variations. The bottom frame shows a low-pressure spectrum, high-pressure conditions are reflected in the middle frame, and intermediate-pressure in the top frame (Reprinted with permission from *Nature*, Copyright 1985 Macmillan Magazines Limited).

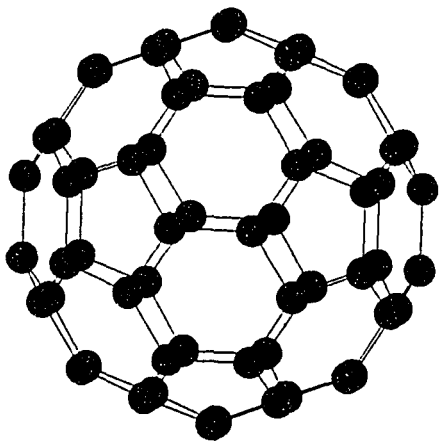

Figure 1.3: The icosahedral structure of C_{60} proposed by Kroto et al. The molecule itself is approximately 1 nm in diameter, including the electron cloud.

Intense interest in the form and properties of stable, high-mass carbon clusters was sparked by the findings of Kroto et al. However, the restriction imposed by finding the clusters exclusively in beam experiments made the availability of new data rare and analysis difficult. The situation was radically changed in 1990 by the discovery [3] of a simple technique to produce macroscopic quantities of these clusters.

The new technique involves the sublimation of graphite in a low-pressure, inert-gas environment. The resulting carbonaceous powder is then harvested and washed with a nonpolar solvent, usually toluene, and the solvent filtered to remove any particulate matter. The liquid thus obtained is reddish to amber colored and contains an entire family of all-carbon, closed-cage molecules known as the fullerenes. The macroscopic samples obtained using this technique were sufficient in size to allow confirmation of the proposed [2] soccer-ball shape of C_{60} and the closed-cage structure of the other fullerenes. The larger versions have been detected

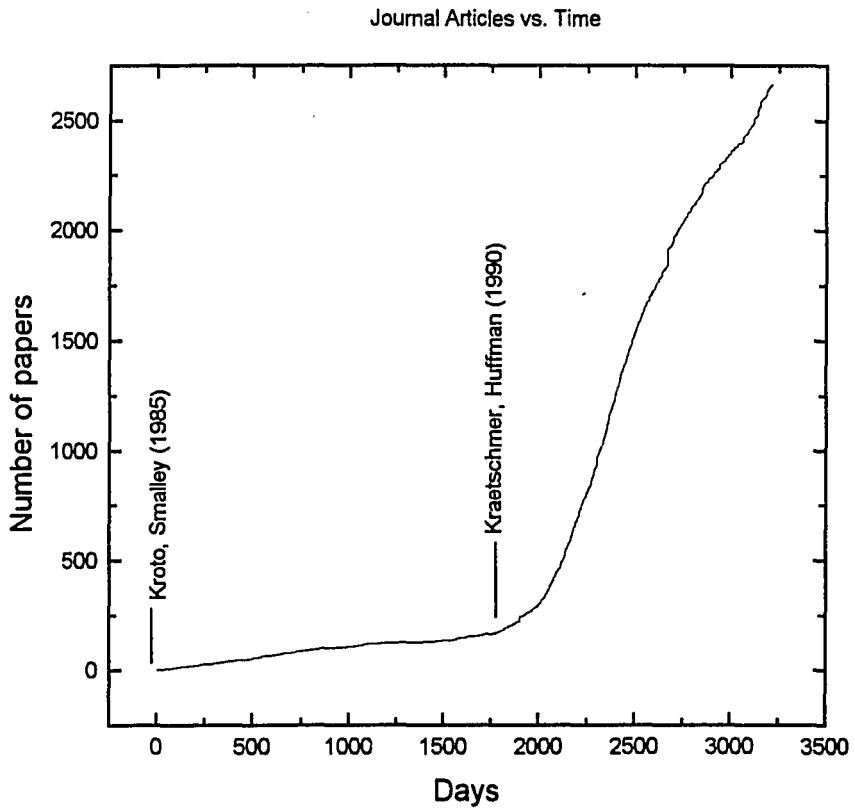

Figure 1.4: An explosion of scientific work on fullerenes, evidenced by the publication count, follows the Krätschmer/Huffman discovery of a method to produce macroscopic quantities of the molecules.

in sizes containing up to 600 carbon atoms.

The explosion of data, theoretical analyses, and new carbon-structure discoveries that the Krätschmer/Huffman fullerene synthesis technique spawned is amply illustrated by Fig. 1.4. The importance of this technique in experimental and future commercial venues testifies to the need for understanding of the processes involved.

1.1 Where are fullerenes found?

Fullerenes have been formed "chemically" in special benzene flames [4] and by pyrolysis of naphthalene [5, 6]. They have been found in natural settings such as Russian coal deposits known as shungite [7], lightning ground-strike remnants called fulgerites [8], and in meteorite craters [9]. Additionally, researchers have produced fullerenes by subliming solid carbonaceous material (graphite, coal, etc.) using electron bombardment [10], RF heating [11], laser vaporization [12], resistive heating [3], and electric arcs [3, 13]. The last two have gained, in the author's view, an unearned distinction, and the terms resistive heating and arc heating are used interchangibly in this text. Of all fullerene sources, the electric arc technique has proven the most commercially viable [14].

As mentioned above, in the Krätschmer/Huffman fullerene production technique, an arc is struck between two graphite electrodes in approximately 100 torr of helium. The resulting soot is washed with a nonpolar solvent, such as toluene, to extract the fullerenes. Since high-yield soot can be obtained by incandescent glowing of the graphite rods [16], the electromagnetic effects, electron/carbon-cluster interactions, and cluster ionization associated with the electric arc seem to have, at best, a minor role in fullerene production. The arc, however, provides more concentrated heating of the rod tips and, thereby, greater sublimation rates.

1.2 How are fullerenes formed?

Despite the large volume of research initiated by the Krätschmer/Huffman process, an actual predictive theory of carbon-sublimation production of fullerenes has yet to be realized. The status that this technique holds in fullerene research demands that its details be determined as accurately as possible. A predictive theory would be invaluable in efforts to maximize efficiency, determine rate and equilibrium constants, establish paths of fullerene formation, and compare production results

from different experimental arc chambers.

Slanina et al. [17], used early energy calculations to show a conflict between the high yield of C_{60} and a state of thermodynamic equilibrium. This group's conclusion that fullerene production was a fortuitous blend of an "adequate temperature-pressure regime" and a "convenient kinetic mechanism" was well supported and underscored the need to examine just what this kinetic mechanism might be.

Four details must be accounted for in any mechanism-specific theory of fullerene formation. One is the the geometric requirement that exactly 12 pentagons must be incorporated into the cage structure to achieve closure [18]. Another is that an energy penalty must be paid if any of these pentagons abut another [18]. Additionally, the C_{60} fullerene fraction must be large, even dominant. Finally, the fullerene yield must be enhanced at increased buffer gas temperatures [13].

The most notable mechanisms are known as the fullerene, pentagon, and ring-zipping roads. The fullerene-road mechanism [19] assumes an initial production of many small, $C_{n<60}$, fullerenes and the addition of C_2 or other tiny C_n fragments to the highly strained, and chemically reactive, fused-pentagon sites, thus expanding the fullerene until a more stable cluster, like C_{60}, is reached. Alternatively, the pentagon-road assumes the growth of graphitic-like sheets, maintaining the least number of dangling bonds at the edges and redistributing pentagons to minimize the sheet energy. Finally, the ring-zipping road assumes the growth, first, of linear, carbon-atom chains which give way to ring-like structures as the number of carbon atoms involved increases. At sizes greater than C_{19} these ring structures can *zip* into the fullerene isomer of that cluster size [23]. An excellent review of these kinetic views, their justification, and possible drawbacks is given by Curl [20].

1.3 This work

The work herein provides experimental data and analysis that reveals linear relationships among the various fullerene abundances resulting from the carbon-arc production technique. The mutual interdependence of these abundances is interpreted as justification for exploring an equilibrium view of fullerene production. Two equilibrium models are then investigated and shown to reproduce important mass-spectrum features.

CHAPTER 2

EXPERIMENT

2.1 Apparatus

With reference to figure 2.5, a horizontal cylindrical chamber with axial electrodes protruding from each end-face served as the foundation for the experimental fullerene production platform. Suitable plumbing allowed evacuation, purging, and controlled gas-introduction. One electrode, although adjustable, remained fixed during the production runs. The other electrode was mounted to a screw-drive apparatus powered by a stepper motor. A Linde^{tm} arc-welder capable of up to 500 amp service served as the power supply. The electrodes (see Fig. 2.6) were constructed of a stainless-steel tube enclosing a smaller brass tube arranged to allow a constant flow of water through the electrode for cooling. The fixed cathode was tipped with a 19 mm-diameter graphite cuff to protect against erosion of the steel. The driven anode was capped with a similar piece of graphite with a hole drilled and tapped on-axis to accept a 6 mm-diameter, 120 mm-long graphite rod intended as feed-stock for fullerene generation. A copper, water-jacket-type heat-exchanger (see Fig. 2.7) inside the chamber, dubbed a shroud, protected the bulk of the chamber interior from the brunt of the arc. The shroud was fitted with an inner sleeve of graphite-cladded copper that could be drilled out longitudinally to allow adjustment of the shroud cooling efficiency.

A pressure sensor on the main water-supply line provided constant flow-rate information while temperature sensors on all water inlets and outlets allowed

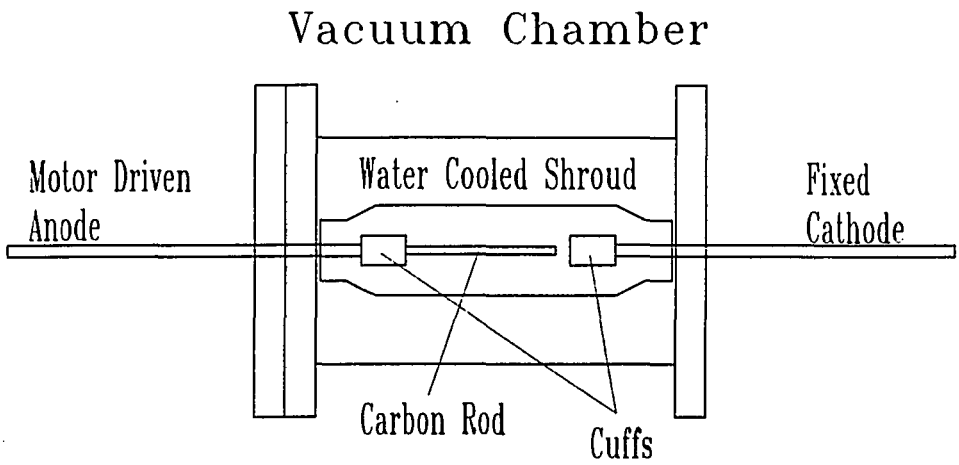

Figure 2.5: The experimental apparatus

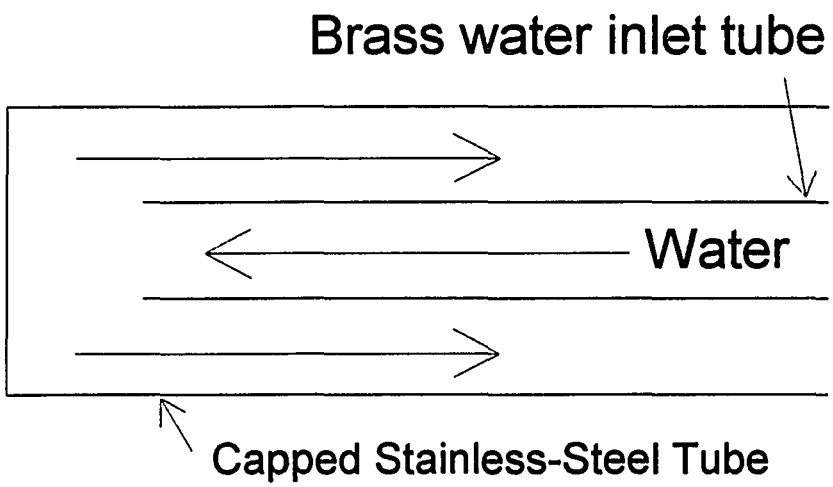

Figure 2.6: Water-cooled electrodes

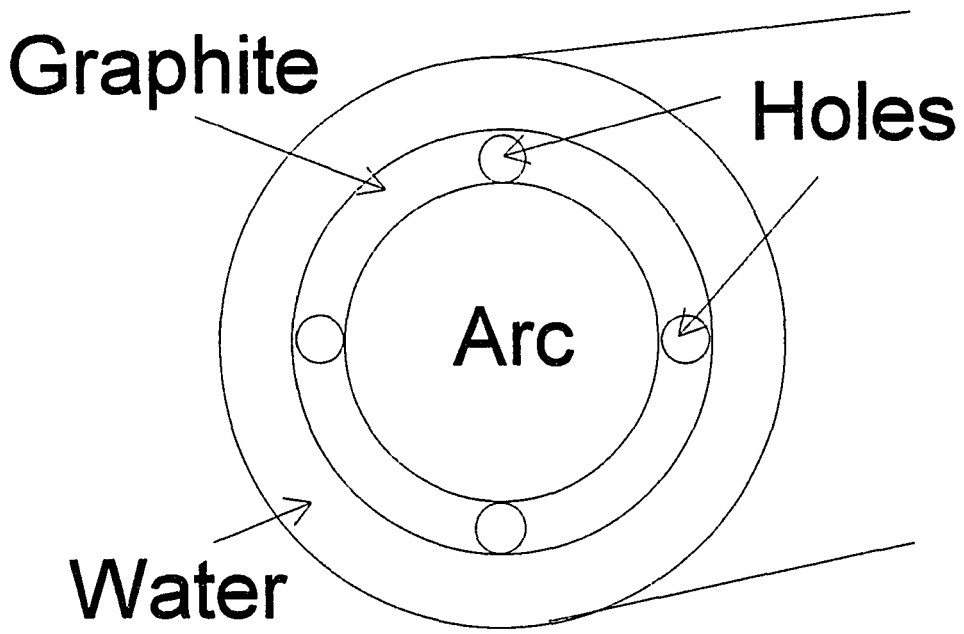

Figure 2.7: Cross-section of water-jacket type shroud showing temperature adjustment holes.

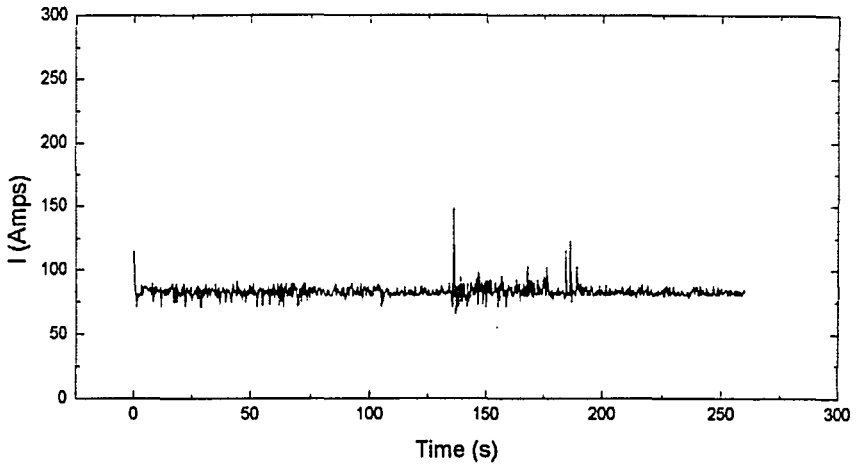

Figure 2.8: Current variation during a 100 mm rod burn.

monitoring of cooling efficiencies. An 83 $\mu\Omega$ shunt allowed analog current monitoring while a Hall-Effect current transducer provided isolated current measurement by computer. Similarly, an analog voltmeter across the arc served the human operator while an induction-based isolation amplifier was used for computer observation of voltage changes. A thermocouple inside the chamber could be used to monitor the temperature of the shroud.

An 80286-based computer acted simultaneously as controller and monitor for the experiments. Software was designed and implemented that allowed electrode-position control based on current feedback. Other feedback parameters were possible, but never tried. Figure 2.8 shows how effectively current levels can be maintained during a 4 minute burn with the computer control.

The bulk of the resistance in the arc circuit is due to the arc gap itself. The second most resistive element is the consumable graphite rod. This means that, as one sublimes the graphite, the resistance of the circuit is reduced substantially. Since the parameter most useful for arc-gap control is the current,

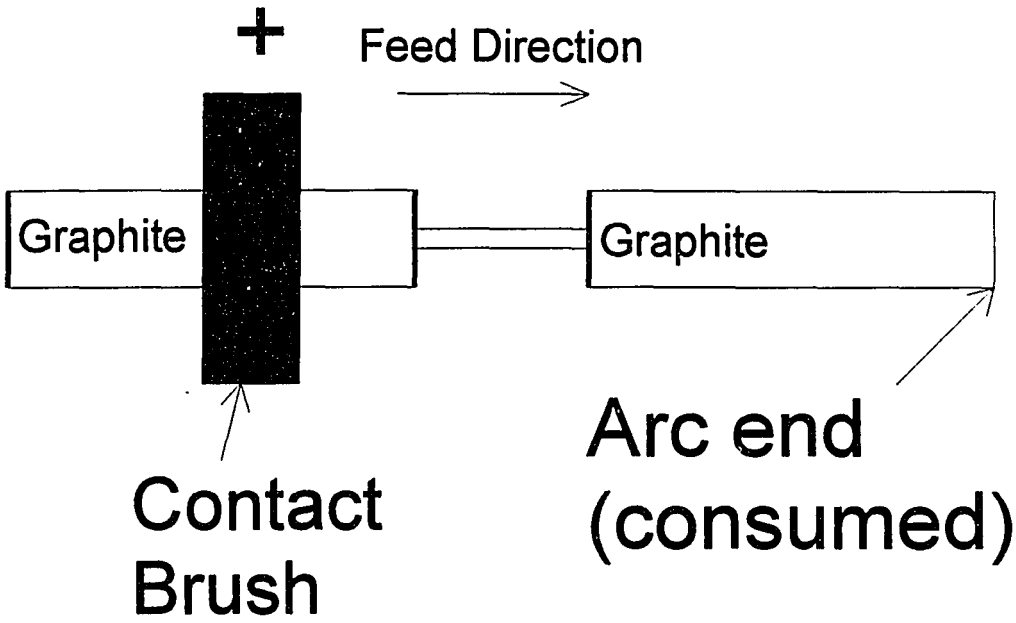

Figure 2.9: Resistance compensation using a second graphite rod.

this constant change in circuit resistance is undesirable. To eliminate the circuit-resistance change due to electrode consumption, a second 6 mm-diameter graphite rod was placed in-circuit and attached to the back end of the anode drive mechanism (see Fig. 2.9). A friction brush arrangement allowed sliding electrical contact with this additional rod assured that the same length of graphite would be in the circuit throughout the burn.

2.2 Procedure

Fullerene production runs were undertaken at 100, 300, and 500 torr of helium, with 3 different voltage settings, and a variety of shroud efficiencies. The procedure was to load a new, consumable 6 mm-diameter, 120 mm-long graphite rod on the anode then close and evacuate the chamber. When the pressure reached $\approx$ 100 microns

(millitorr) of mercury the chamber would be back-filled with helium to $\approx$ 600 torr and then reevacuated to 100 microns again. Helium would then be added until the desired working pressure was obtained. Power, at the desired setting, would then be applied to the electrodes and the system put under computer control. The computer program would advance the anode to strike the arc and then withdraw to achieve a 1.5 *mm* arc length. The current would then be logged and incremental changes in anode position used to maintain this current, and, thereby, the desired arc-gap.

. The evaporated carbon from each run was harvested from the powder-covered surfaces of the chamber with a paint brush and passed through a 7 wire-per-cm screen to separate large chunks from the fine soot. The soot from the shroud interior and that from the rest of the chamber were kept separate. A small, $\approx$ 8 mg, sample of soot from each of the two regions was carefully weighed on a microgram balance and toluene added to make a 1 mg/ml soot-to-toluene slurry. This mixture was placed in an ultrasonic cleaner for $\approx$ 5 minutes and then poured through a number 42 Whatman paper filter. The resulting amber liquid was poured into a glass cuvette and then placed in a Cary 118 spectrophotometer. Absorption as a function of wavelength from 350 nm to 800 nm was recorded by computer for each sample and then analyzed by generalized least-squares curve-fitting to known, mass-normalized C_{60}, C_{70}, C_{76}, C_{78}, and C_{84} absorption spectra (see Appendix 1). These constituents are known to comprise $>$ 99% of the fullerenes present in the soot [34].

Fullerene yield was computed as the total fullerene concentration in mg/ml, as measured via the optical absorption technique, divided by the original 1 mg/ml soot-to-toluene slurry concentration.

Once all pressure/power-setting combinations were completed, part of the graphite cladding on the inner shroud sleeve was removed by drilling. This was done to reduce the cooling efficiency of this element and, thereby, change the

temperature profile in the chamber during the subsequent burns.

After the systematic production study was completed, various techniques were tried in an attempt to maximize yields. These included placing a graphite tube inside the shroud with small "feet" to minimize thermal conduction between this tube and the shroud. This further probed the fullerene yield dependence on the temperature profile in the chamber.

Another yield maximization technique tried, was to allow helium to flow during the burn in order to maintain a cleaner environment. It is well known that atmospheric contaminants have a deleterious effect on fullerene yield [14]. This technique was meant to circumvent a leakage problem if one existed.

CHAPTER 3

RESULTS

The experimental study of fullerene production dependence on various parameters provides little new information. Figure 3.10 shows the gross behavior reported by other groups [14], i.e., yield, defined as milligrams of fullerenes extracted per milligram of soot, reaches a maximum at lower He pressures. Focusing on the high-yield, 100-torr-pressure studies, figures 3.11-3.13 show total fullerene yield versus applied voltage, current, and power. No predictable relationship between fullerene yield and these parameters is apparent. The yield versus temperature-profile studies similarly showed no apparent relationship between fullerene yield and shroud efficiency.

There was a small difference between the soot harvested from the interior of the shroud and that from the rest of the chamber. The shroud soot was usually a few percent less abundant in fullerenes. This is assumed to be due to the low sublimation temperature of the fullerenes as compared with the other constituents in the soot. The fullerenes simply moved out of the shroud. It is also possible that the brunt of the arc on the soot inside the shroud served to destroy the fullerenes there.

The ability to determine species yields for C_{60}, C_{70}, C_{76}, C_{78}, and C_{84} from the UV/visible absorption spectrum of the extract leads to several new results. Figure 3.14 shows that a linear relationship between total fullerene yield and C_{60} yield exists over a wide range of conditions. Further, figures 3.15-3.18, showing C_n fractions, defined as the C_n yield divided by the total fullerene yield, indicate that

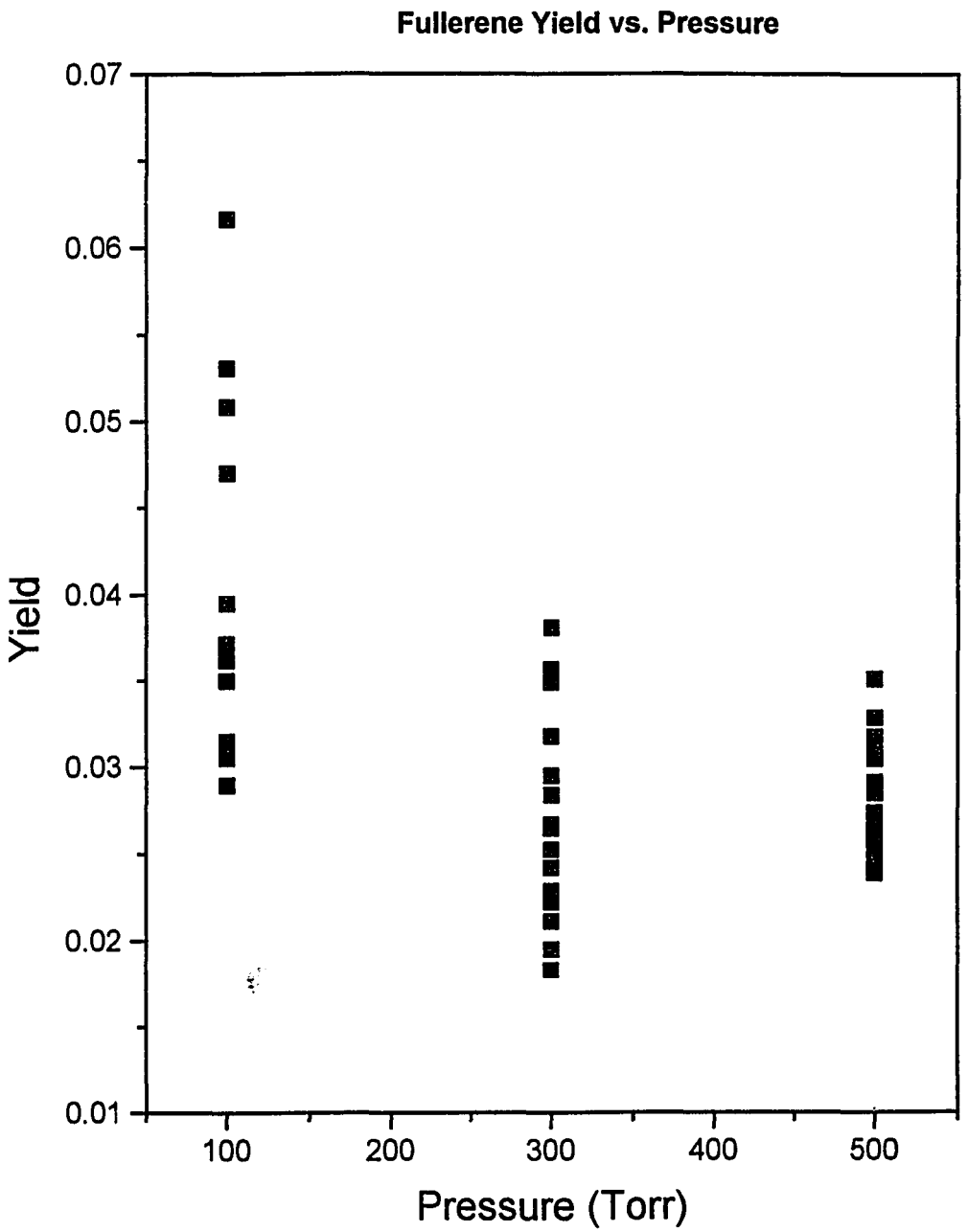

Figure 3.10: Total fullerene yield, defined as milligrams of fullerenes extracted per milligram of soot, as a function of He pressure.

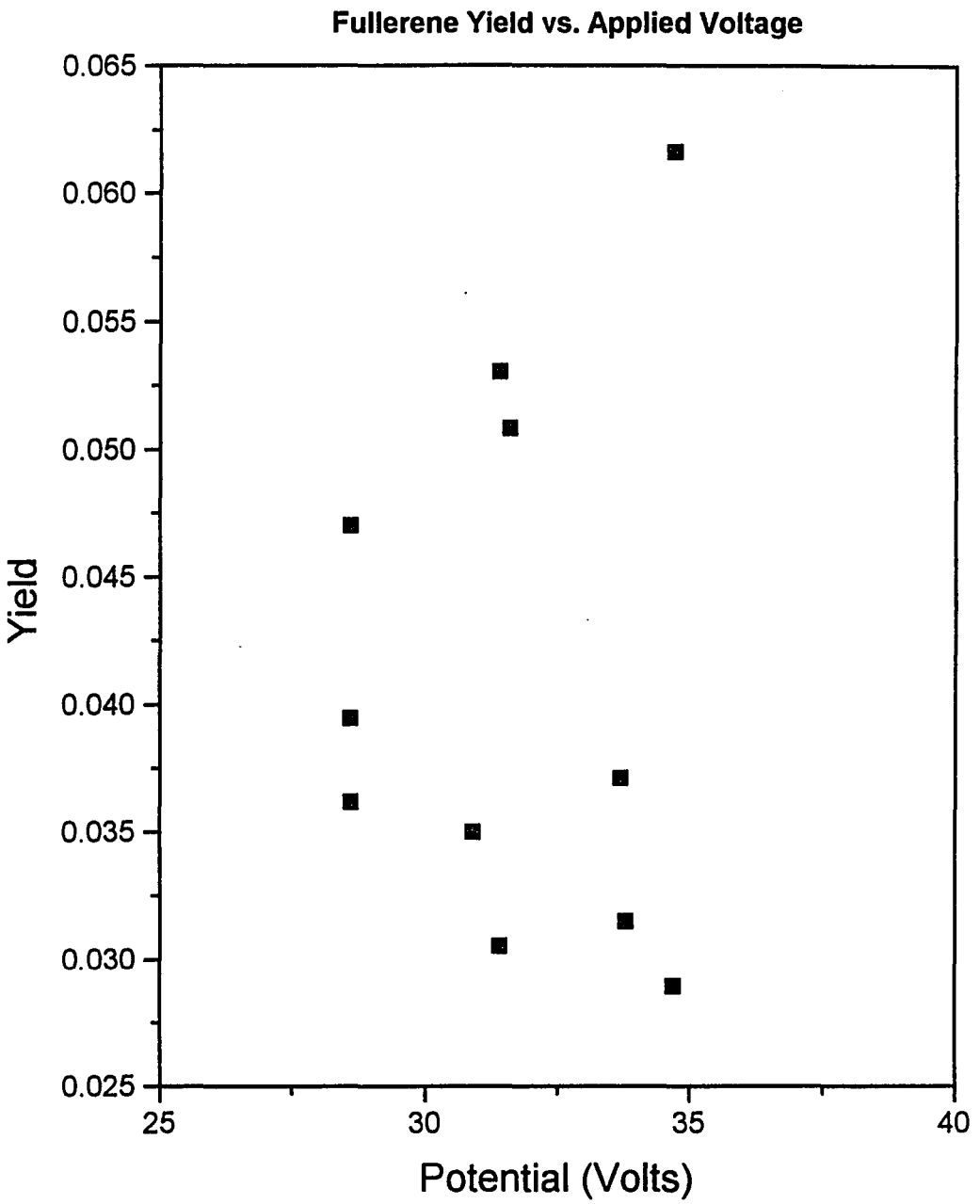

Figure 3.11: Total fullerene yield, defined as milligrams of fullerenes extracted per milligram of soot, as a function of applied voltage. The He pressure for these runs was maintained at 100 torr.

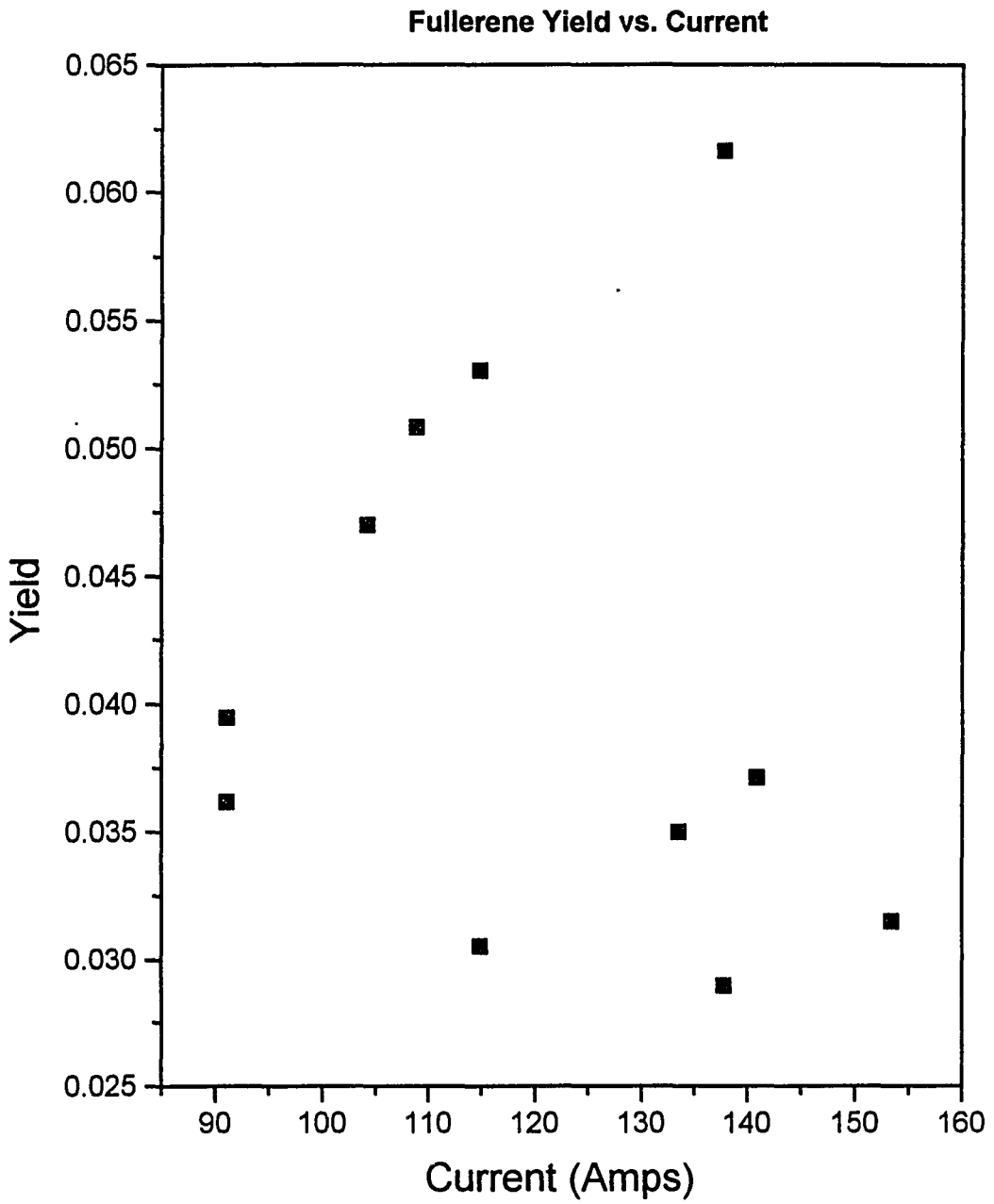

Figure 3.12: Total fullerene yield, defined as milligrams of fullerenes extracted per milligram of soot, as a function of current flow. The He pressure for these runs was maintained at 100 torr.

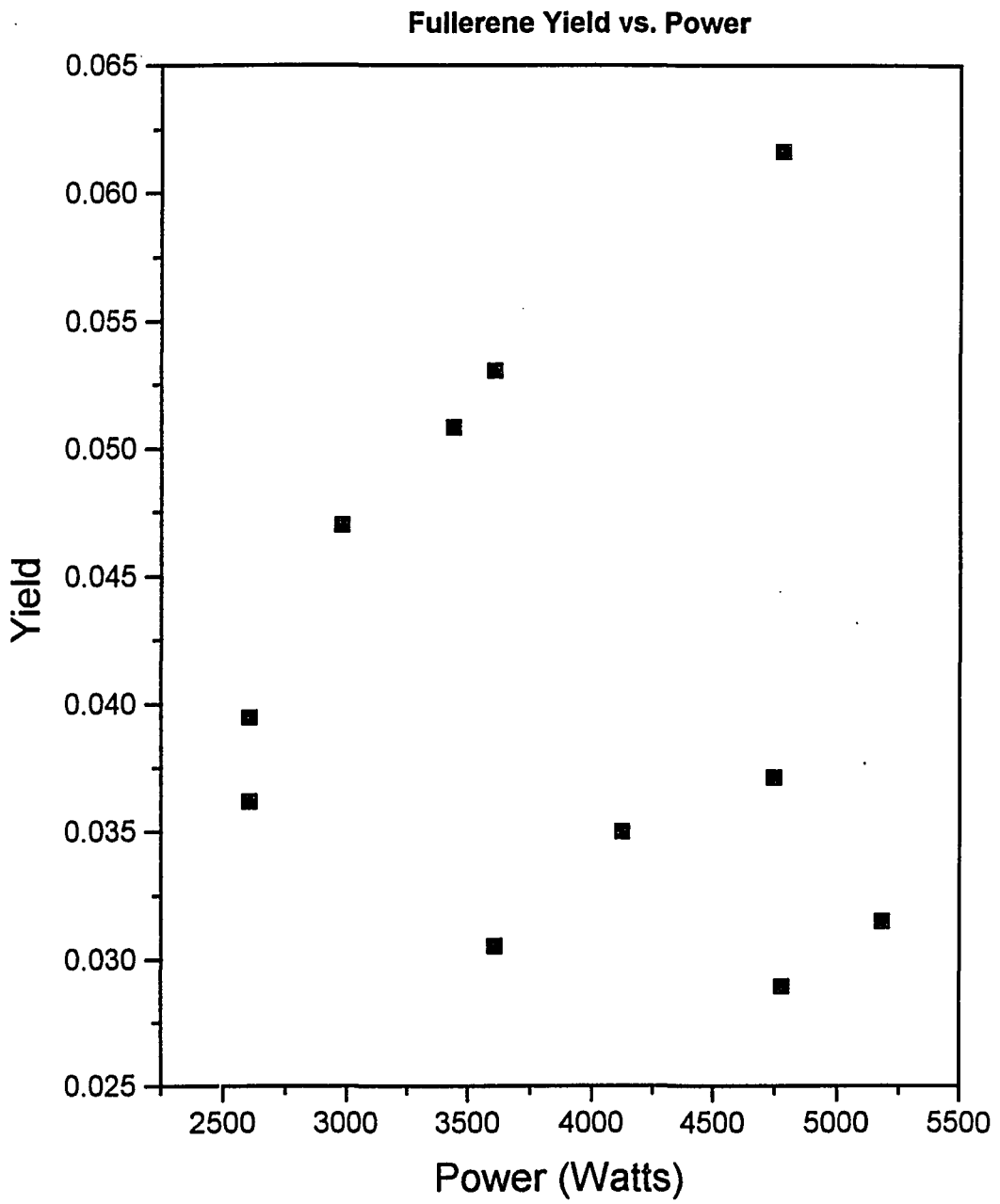

Figure 3.13: Total fullerene yield, defined as milligrams of fullerenes extracted per milligram of soot, as a function of power dissipated. The He pressure for these runs was maintained at 100 torr.

linear relationships exist among all the species tracked.

The helium-flow burns showed little change in yield until the helium inlet position was moved. By positioning the helium inlet so that the gas would flow down the inside of the shroud, a two-fold increase in fullerene yield was obtained. The direction of flow down the shroud made little difference; both directions gave increased yield. Other inlet positions were attempted, but no further improvement was achieved.

Future experiments with the production chamber required holes to be drilled horizontally through the shroud to allow direct viewing of the arc. This modification coupled with helium flow, now directed at these holes, and a large (7 mm) arc gap, resulted in the highest repeatable yields to date—25%. The longer gap decreases the current flow and, thereby, the graphite sublimation rate. Burns of greater than 20 minutes are required to consume 100 mm of rod. The maximum yield conditions to date are: 100 torr helium, gas flow during burn, 7 mm gap, and 75 amps.

The data resulting from high-yield conditions are included in figures 3.14-3.18 with different symbols. Even though these runs had marked differences in yield, gap, configuration, and duration, compared with the more systematic study, the linear relationships among the constituents still apply.

3.1 Discussion

The relationships shown in Figs. 3.14-3.18 have not been reported elsewhere. They seem to provide a useful technique to determine species fractions if the total yield is known. Equivalently, if one species yield is known, all others, and the total yield, can be determined. Linear regression fits to the data give the following equations for determining species fractions in terms of the total yield:

$$C_{60} = 0.70 - 0.0094/Y_T$$

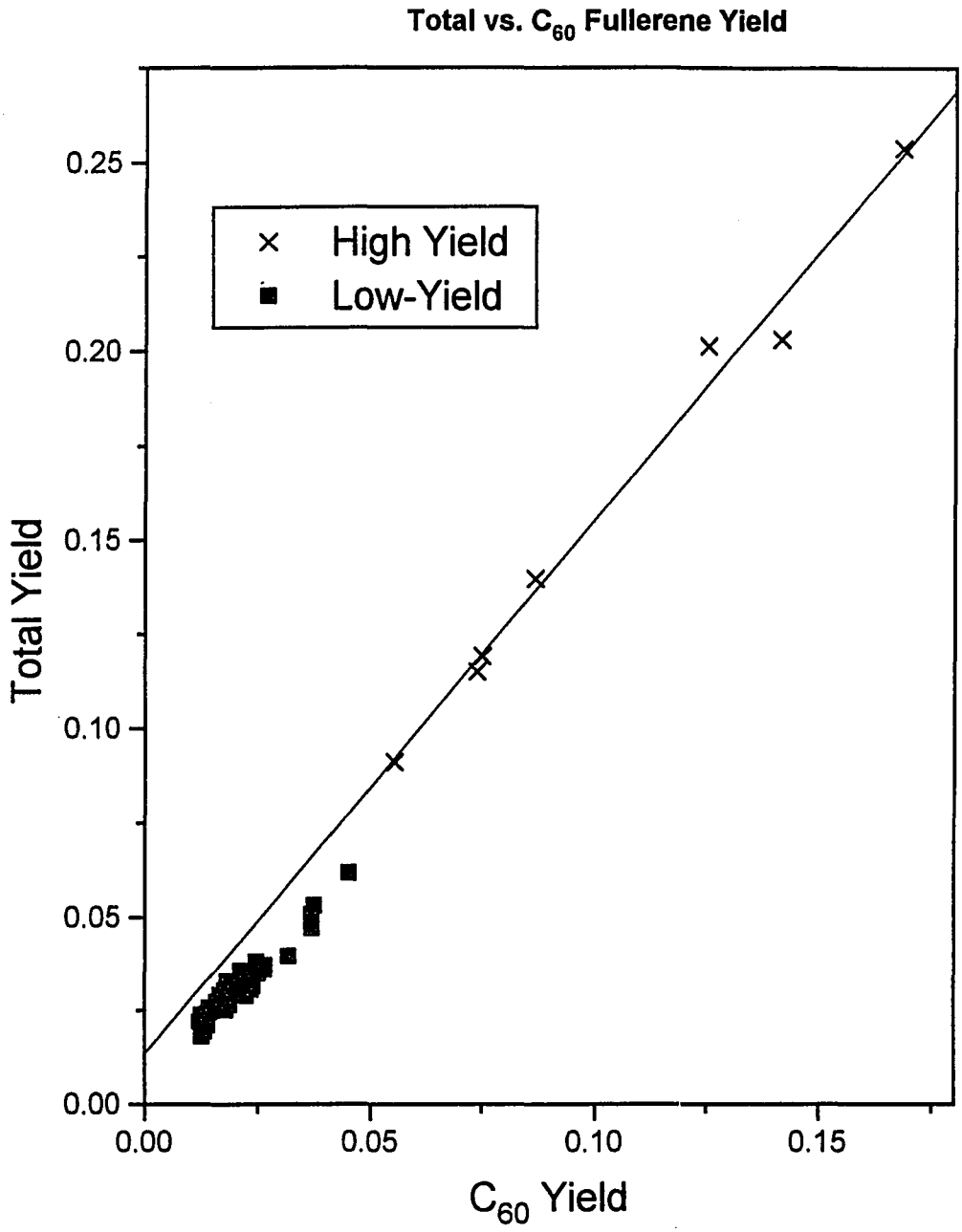

Figure 3.14: Total fullerene yield, defined as milligrams of fullerenes extracted per milligram of soot, as a function of C_{60} yield. Data represent runs where pressure, applied voltage, shroud efficiency, burn duration, and flow configuration were varied.

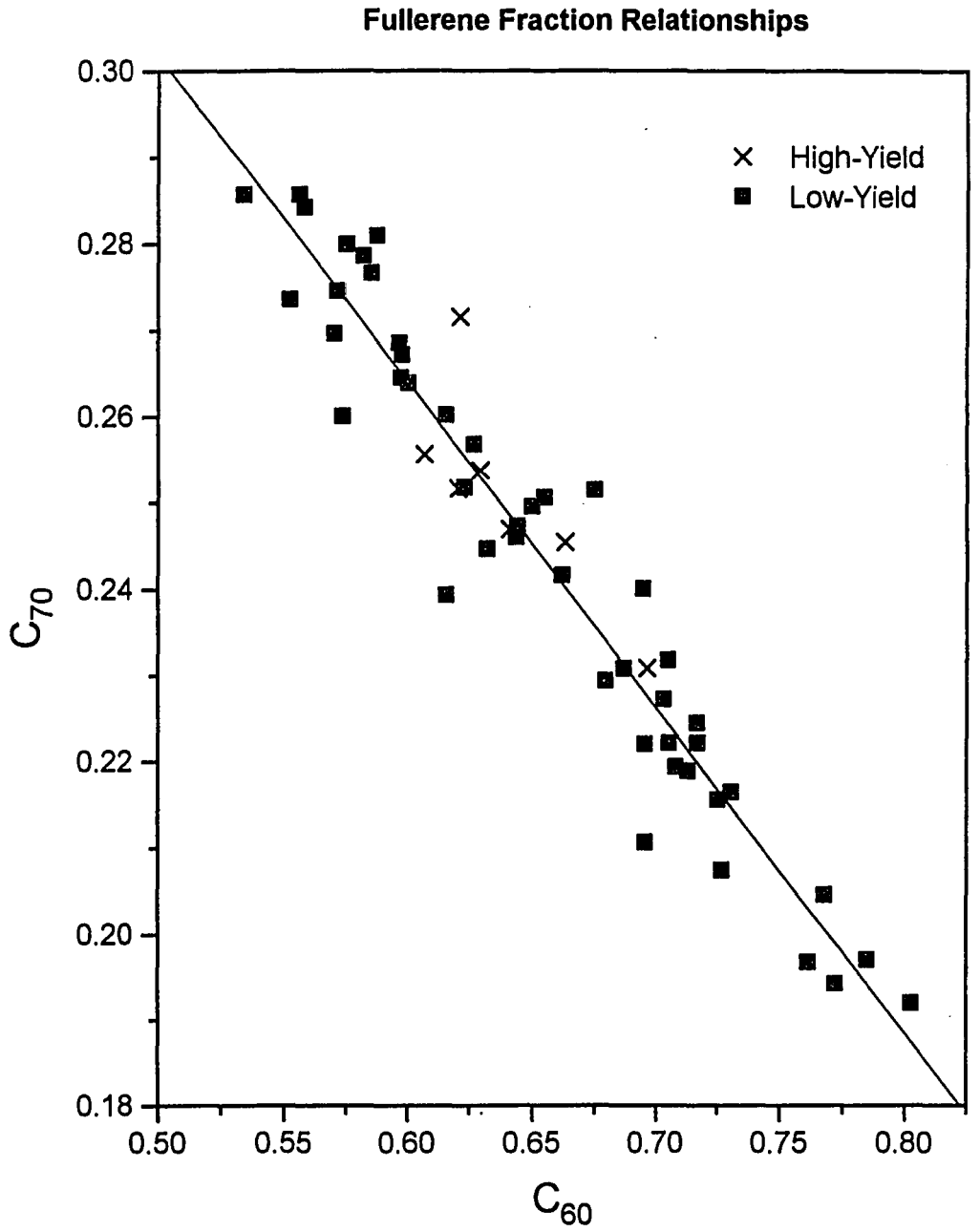

Figure 3.15: C_{70} versus C_{60} fractions, defined as the ratio of C_n concentration to the total fullerene concentration in extract. Data represent runs where pressure, applied voltage, shroud efficiency, burn duration, and flow configuration were varied.

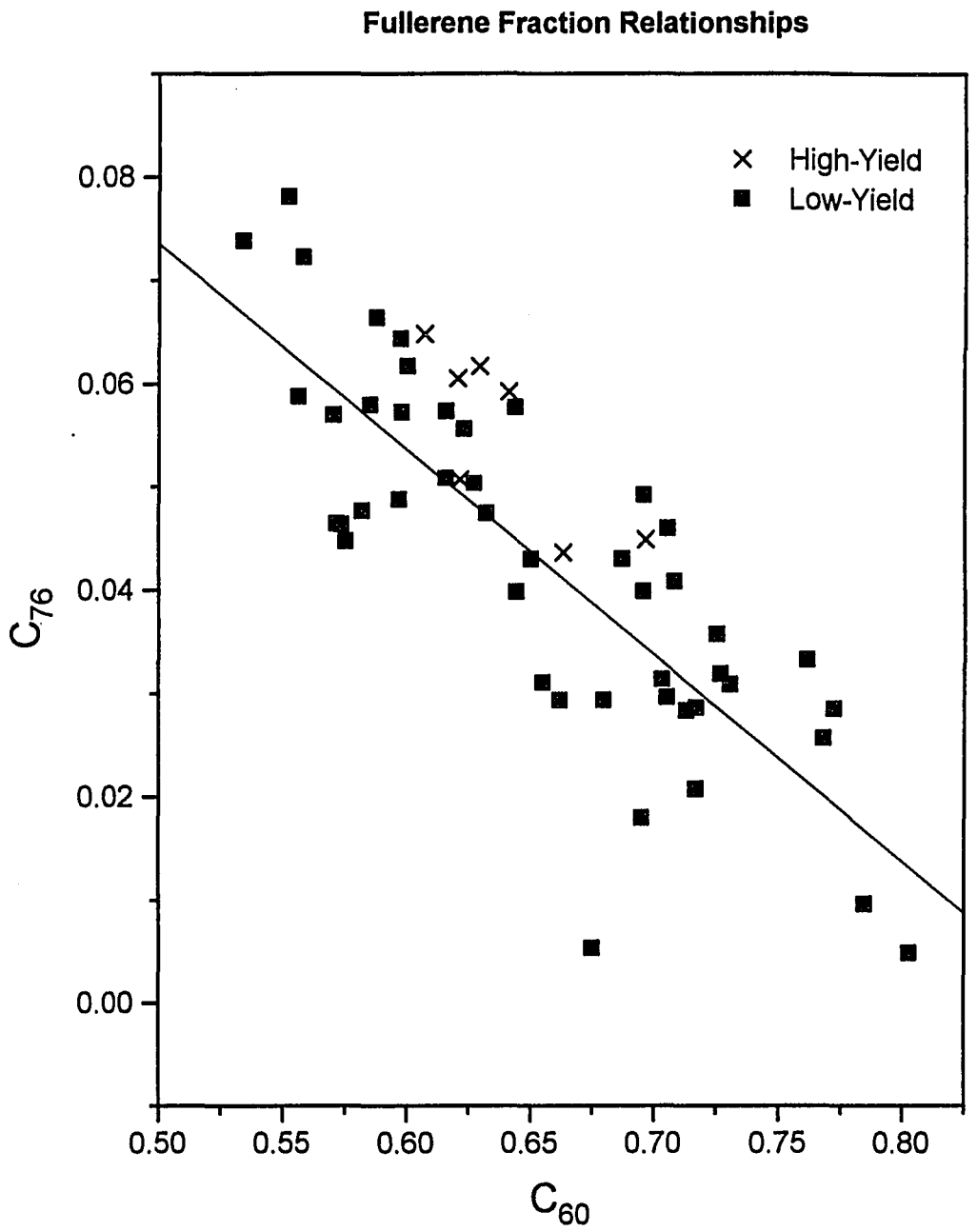

Figure 3.16: C_{76} versus C_{60} fractions, defined as the ratio of C_n concentration to the total fullerene concentration in extract. Data represent runs where pressure, applied voltage, shroud efficiency, burn duration, and flow configuration were varied.

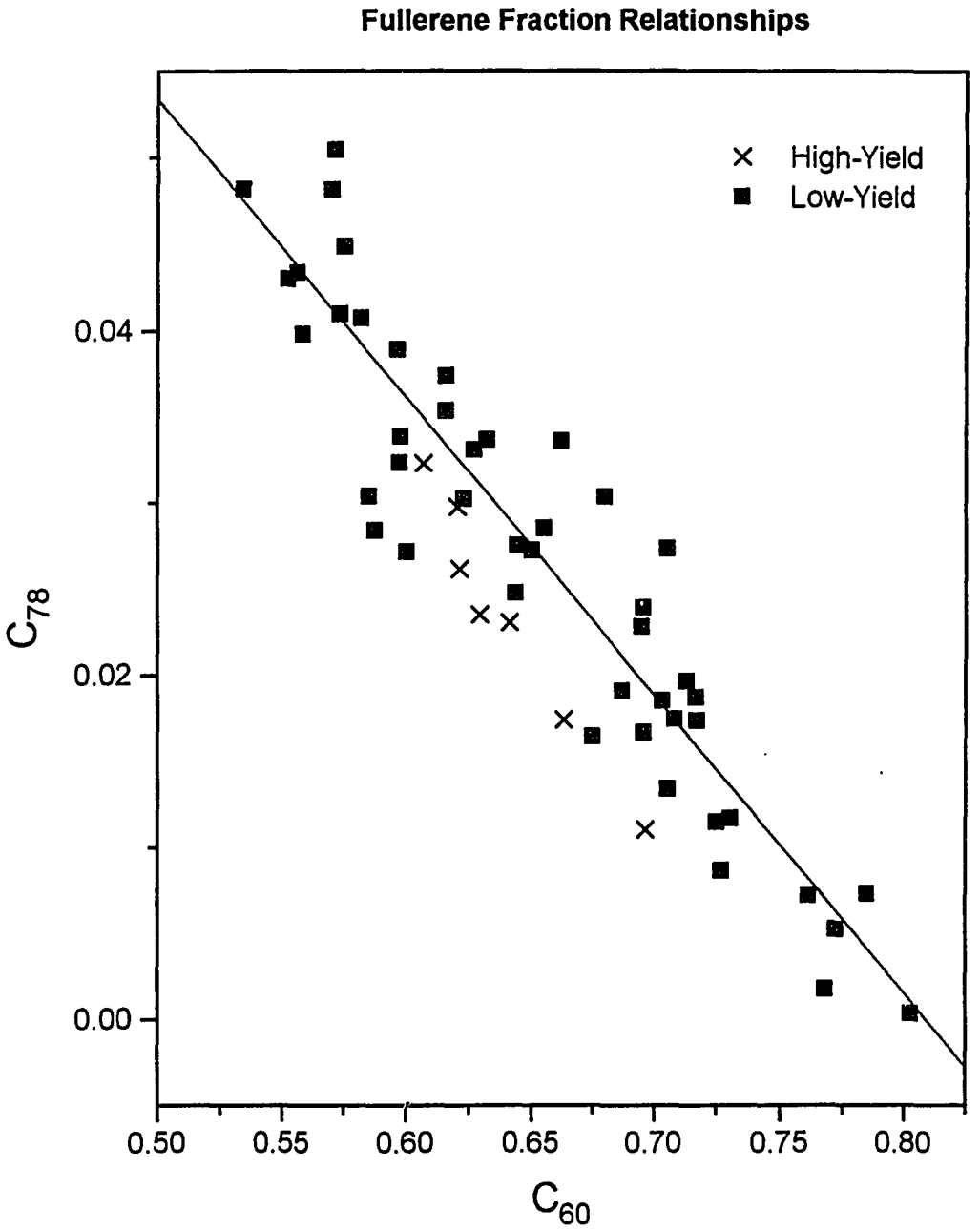

Figure 3.17: C_{78} versus C_{60} fractions, defined as the ratio of C_n concentration to the total fullerene concentration in extract. Data represent runs where pressure, applied voltage, shroud efficiency, burn duration, and flow configuration were varied.

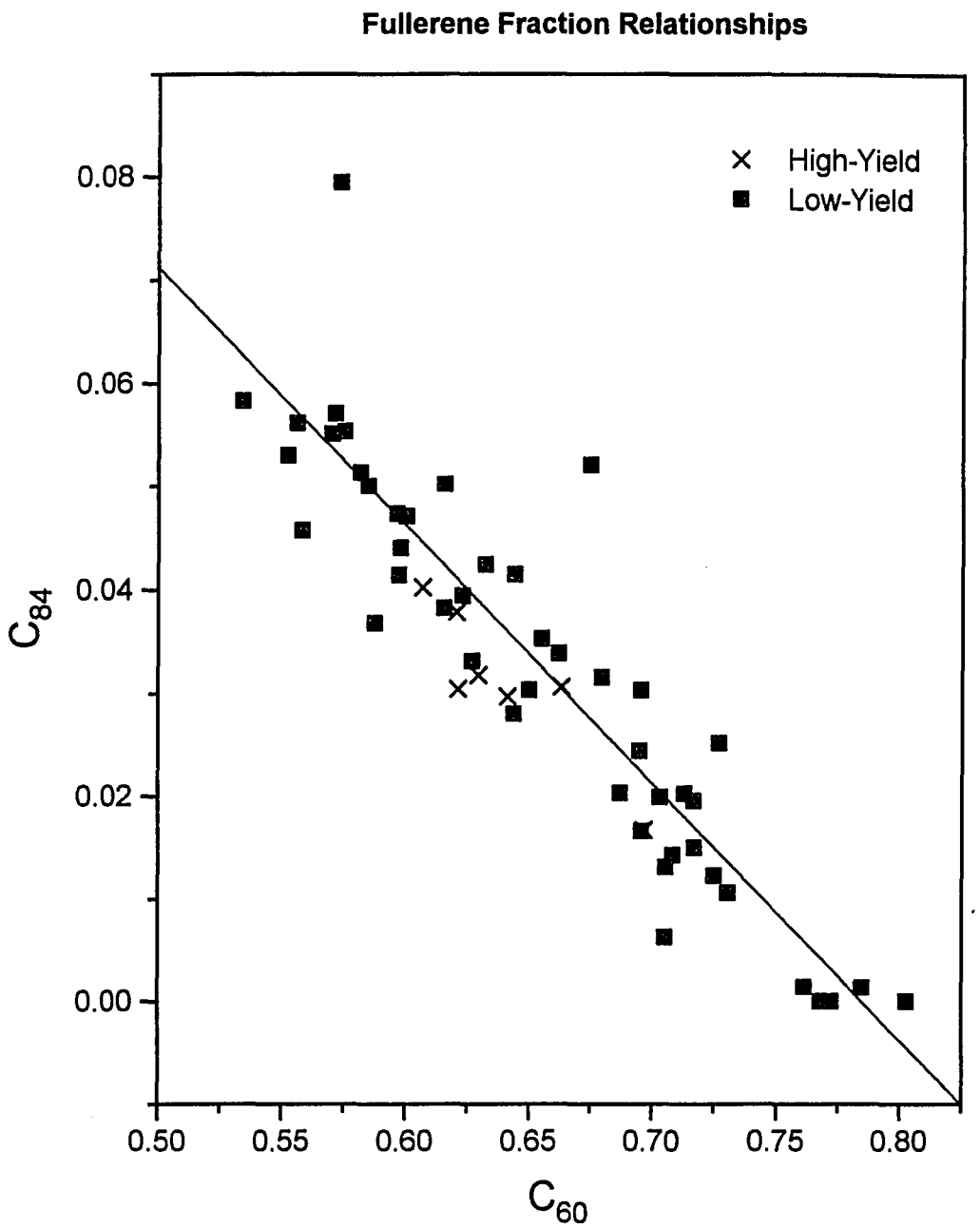

Figure 3.18: C_{84} versus C_{60} fractions, defined as the ratio of C_n concentration to the total fullerene concentration in extract. Data represent runs where pressure, applied voltage, shroud efficiency, burn duration, and flow configuration were varied.

$$
\begin{aligned}
C_{70} &= 0.22 + 0.0036/Y_T \\
C_{76} &= 0.03 + 0.0019/Y_T \\
C_{78} &= 0.021 + 0.0016/Y_T \\
C_{84} &= 0.025 + 0.0024/Y_T,
\end{aligned} \tag{3.1}
$$

where Y_T represent the total yield.

The concentration of a particular species is given by the product of the number produced and the solubility of that product given the presence, in both cases, of other species. This means that the above relations are not necessarily a statement just of production values.

The yield increase due to helium flow down the inside of the shroud is reminiscent of the report by Parker et al. [15] that yield increases were seen after placing shims in the production chamber and Haufler et al. [13] that a "chimney" above the arc provides better yields. In our case the effect would be to lower the temperature where the shim placement would serve to increase the production region temperature. This indicates that the effect isn't due to temperature changes. However, in all cases the turbulence patterns near the arc would be altered. It is this turbulence effect that is a likely candidate for the yield changes.

A possible explanation for turbulence affecting yield is that molecules are intercepted as they diffuse outward from the electrode evaporation region and further reactions are quenched. This would seem to indicate that, beyond a point, reactions tend to reduce fullerene yield as opposed to increasing it as one might expect.

Beyond just being a technique of analysis, the linear relationships among the species fractions seem to show a common, or at least related, production basis for all fullerenes. Such a relationship, considering the large number of species and related bonds involved, should have a statistical description. The aim in the next chapter is to explore an equilibrium description of fullerene formation.

CHAPTER 4

THEORY

Carbon-evaporation fullerene-production enjoys widespread use in both the commercial and experimental arenas. A useful analytical description of the process, however, has not been forthcoming. Figure 4.19 shows a typical example of the mass spectrum of fullerene-laden soot produced through the popular Krätschmer-Huffman carbon-arc process. The features to note are the C_{60}-peak dominance, the rapid decay toward higher cluster numbers, and the C_2 spacing between the peaks. Any theory of fullerene production must predict these features to be successful. Prompted by the experimental results that seem to indicate a possible equilibrium view of fullerene formation, outlined here is a description that predicts salient mass spectrum features, i.e., species-relative yields, overall yields, and even-cluster dominance.

After a brief review of the thermodynamics of chemical equilibrium, it will be shown that the simple chemical statement

$$nC_1(s) \rightarrow \frac{1}{4}C_{n,linear} + \frac{1}{4}C_{n,ring} + \frac{1}{4}C_{n,sheet} + \frac{1}{4}C_{n,fullerene}(= C_n), \qquad (4.2)$$

assuming equilibrium, provides cluster abundances shown in Figs. 4.21-4.27, effectively reproducing the features mentioned. In the process, simple Gibbs free energy relations for linear, ring, sheet, and fullerene isomers of n-atom-sized carbon-clusters will be found. These relations will be used in the equilibrium-based analysis.

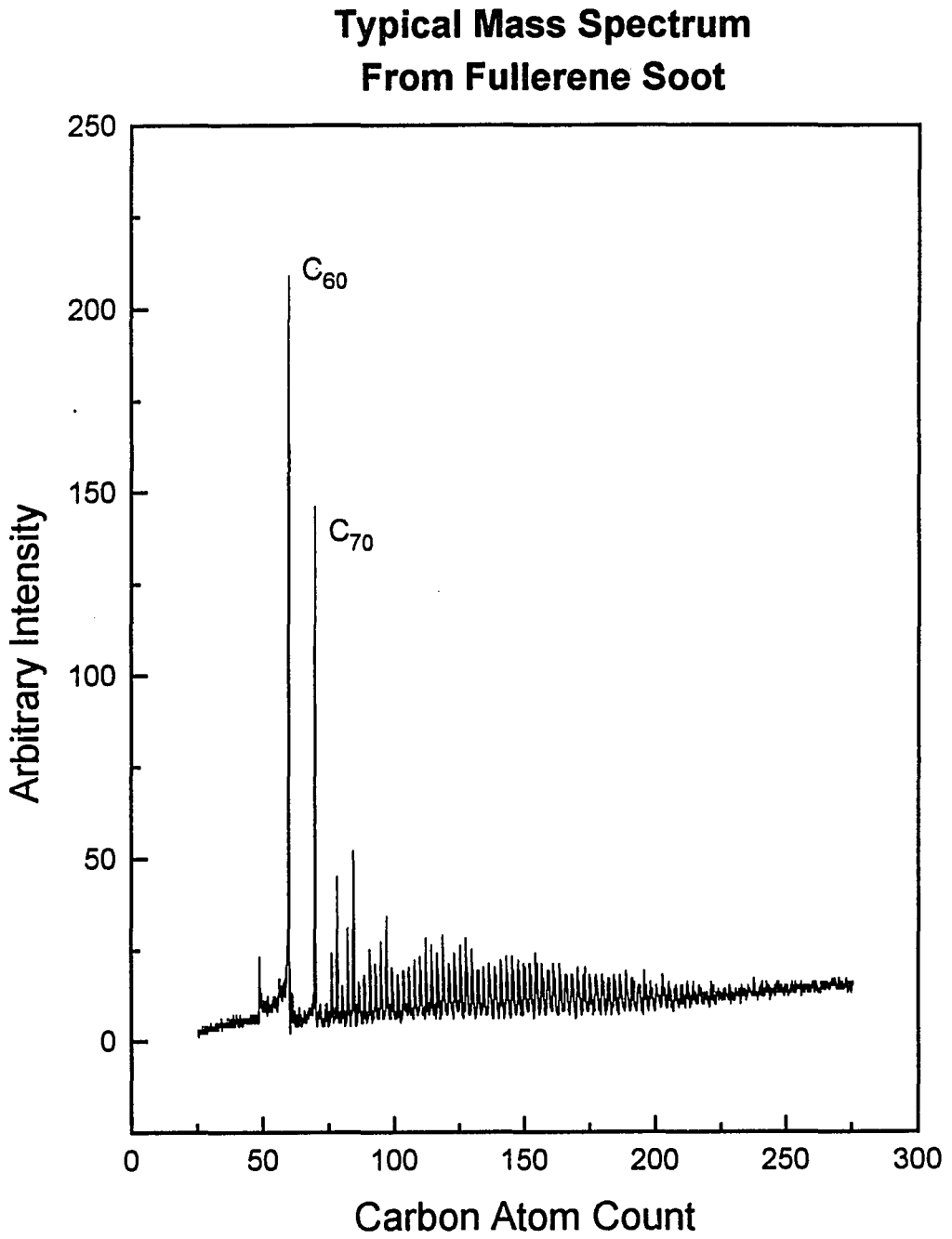

Figure 4.19: Typical mass spectrum of CS_2 extraction of fullerene-bearing soot. (Courtesy of Michael Zumwalt)

4.1 Thermodynamics of equilibrium

Recall that the Gibbs free energy of a system of particles is defined as

$$G = E - TS + pV,$$

or

$$\begin{aligned} dG &= dE - TdS - SdT + pdV + VdP \\ &= -SdT + VdP. \end{aligned} \tag{4.3}$$

So, for a system evolving under constant temperature conditions,

$$dG = VdP.$$

For an ideal gas, this becomes

$$dG = RT\ d(\log P),$$

or

$$\Delta G = RT\ \log \frac{P}{P_0},$$

where R is the gas constant and P_0 is the reference-state pressure. Note that we are dealing with ΔG *per mole* in these equations.

A chemical reaction,

$$\nu_1 B_1 + \nu_2 B_2 + \ldots + \nu_n B_n \rightarrow \nu_{n+1} B_{n+1} + \nu_{n+2} B_{n+2} + \ldots + \nu_N B_N,$$

can be equivalently written

$$\sum_i \nu_i B_i = 0,$$

where, by convention, the product coefficients are positive and the reactant coefficients are negative. For example,

$$2H_2 + O_2 \rightarrow 2H_2O$$

can be written

$$2H_2O - 2H_2 - O_2 = 0,$$

where

$$\begin{aligned} \nu_1 &= 2 \\ \nu_2 &= -1 \\ \nu_3 &= -1 \\ B_1 &= H_2O \\ B_2 &= H_2 \\ B_3 &= O_2. \end{aligned} \tag{4.4}$$

For an ideal gas system undergoing a chemical reaction described by

$$\sum_i \nu_i B_i = 0,$$

the change in free energy for the system is given by

$$\begin{aligned} \Delta G &= \sum_i \nu_i \Delta G_i \\ &= \sum_i \nu_i RT \ log \frac{P_i}{P_{i,0}} \\ &\equiv \sum_i \nu_i (\Delta G_{i,0} + RT \ log P_i), \end{aligned} \tag{4.5}$$

where $\Delta G_{i,0}$ is the Gibbs energy to put species i into a reference, or standard, state, and P_i is the partial pressure of the ith component. The condition for equilibrium is [21, 22],

$$\Delta G = 0,$$

or, using Eqn. 4.5,

$$\begin{aligned} \log \left(\prod_i P_i^{\nu_i} \right) &= -\sum_i \nu_i \Delta G_{i,0}/RT \\ &\equiv \log K_p, \end{aligned} \tag{4.6}$$

where K_p is the equilibrium constant of the reaction.

Using Eqn. 4.6, known values of standard-state Gibbs energies for all our components, and a set of reaction equations, we can determine the partial pressures of components in a gas. In what follows we will be choosing particular stoichiometric equations to represent the carbon-cluster chemistry occurring under fullerene production conditions. Note, however, that the specification of the reaction equations determines the outcome of our partial pressure calculations. There are an infinite number of stoichiometric equations that can be written down for any multicomponent system. As long as the equations are balanced, i.e., mass and charge are not created or destroyed, they are valid. The chemical process they describe, however, may never occur.

4.2 Gibbs energies for various cluster isomers

Evaluation of the equilibrium relationship(s) given by Eqn. 4.6 require that we first determine the Gibbs energies for a representative sample of carbon-cluster isomers. We'll use linear chains, mono- and poly-cyclic rings, graphitic fragments, and fullerenes as our representative isomers, as suggested by ion chromatography experiments [23, 24] and the primarily graphitic nature of the soot. Note that all energies will be given in eV.

As one would expect, the first attempts to analyze the relative abundances of the various cluster sizes in the mass spectra involved the measurement [25, 26] and calculation [27, 28] of cluster binding energies for the fullerenes. Tersoff [27] used geometrical bending strain arguments to arrive at possibly the most useful theoretical description of fullerene energies. For a fullerene cluster of n atoms, the energy, given as a cost per pentagon, is

$$E_5 = \lambda_5 + \beta_5 ln(n/60).$$

Ab initio calculations give the value of λ_5 and β_5 as 3.36 and 0.61, respectively.

The measured [25, 26] and tight-binding model calculation [29] value of λ_5 is considerably less—2.1 and 2.0, respectively. For the remainder of this chapter, the experimental value of λ_5 will be assumed and the energy per fullerene computed using

$$E = 25.2 + 7.32ln(n/60), \tag{4.7}$$

where the Euler requirement for 12 pentagons accounts for the additional factor. Note that this is an energy over that of graphite. An infinite-sized fullerene can be seen as an infinite sheet of graphite with 12 minor pentagonal defects. This notion leads to the estimation that the Gibbs energy for fullerenes is simply that of graphite adjusted by the Tersoff potential.

We now turn our attention to the Gibbs energies for linear chains. Tabular data [30] of small carbon-cluster equilibrium constants show the expected T^{-1} dependence as in Fig. 4.20. Linear regression analysis of this tabular data provides the following set of equations:

$$\begin{aligned} log(K_2) &= -6.45 + 2.73/kT \\ log(K_3) &= -13.6 + 5.95/kT \\ log(K_4) &= -20.8 + 8.29/kT \\ log(K_5) &= -27.9 + 11.44/kT, \end{aligned} \tag{4.8}$$

where the subscript numerals refer to the carbon-cluster size. These data are for the chemical processes

$$nC_1 \rightarrow C_n.$$

These are remarkably well fit by the relation

$$\log(K_n) = 7.9 - 2.87/kT + n(-7.2 + 2.85/kT),$$

i.e.,

$$\Delta G_n = (-7.9 + 7.2n)kT + (2.87 - 2.85n). \tag{4.9}$$

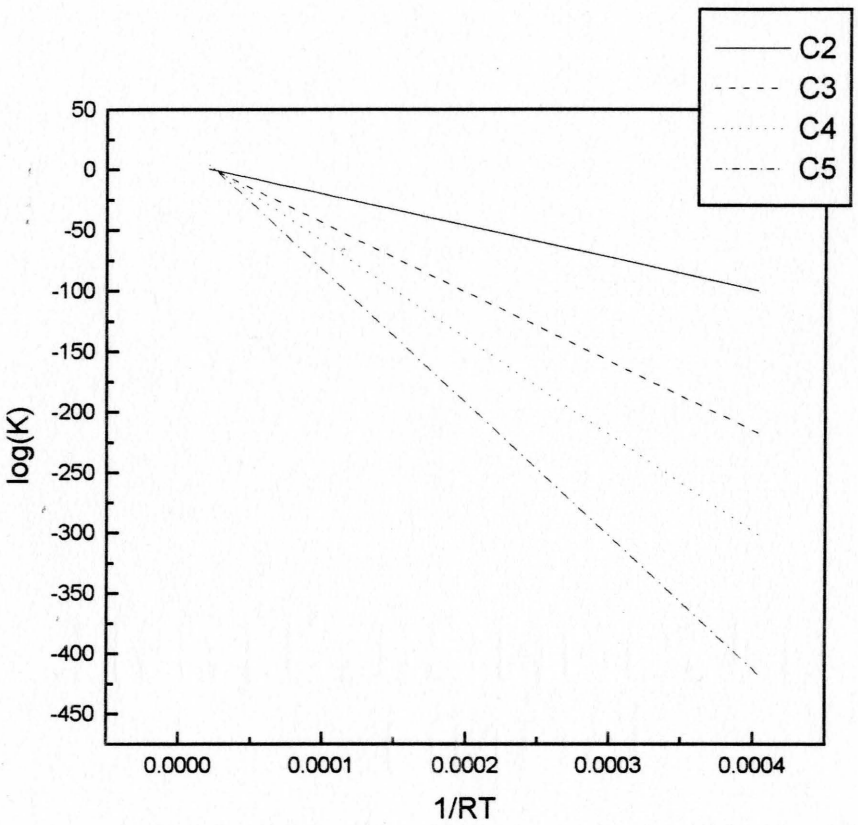

Figure 4.20: log(K) values for small C_n clusters from tables.

Studies have shown conclusively [24, 31], however, that odd and even small clusters behave differently. The accurate linear fit to the set of both types of clusters and the odd/even differences reported widely in the literature suggest that a separate linear fit for odd and even structures would be more accurate in representing their respective energies. This analysis leads to the following representations of the energies for linear chains:

$$\begin{aligned} G_{n=2j} &= (-7.9 + 7.2n)kT + (2.84 - 2.78n) \\ G_{n=2j+1} &= (-7.9 + 7.2n)kT + (2.29 - 2.75n). \end{aligned} \tag{4.10}$$

The splitting of odd and even carbon clusters into two groups based on the energy relationships among the members of the group is not unprecedented. Raghavachari and Binkley in reference [31] find a linear relationship among small, odd-numbered carbon-cluster binding-energies and specifically note the odd-even differences found in their calculations. In addition, the linear dependence on cluster size, n, of binding energies and entropy changes for small carbon clusters ($n \leq 10$) was previously reported by Pargellis [32]. The extension made here is to combine the two effects by assuming a separate linear dependence on n for odd and even clusters that holds over a broad range of cluster sizes.

Equivalent $\log(K)$ data for graphite gives the following

$$G_1 = (8.14kT - 3.23). \tag{4.11}$$

Note that this is for a single carbon atom in graphite going to the gas phase,

$$C_1(s) \rightarrow C_1(g).$$

The graphitic fragment isomer, which is referred to as a sheet, consisting of n carbon atoms will have a Gibbs energy of graphite adjusted by the number of dangling bonds at the edges. By assuming a circular fragment, the number of dangling bonds will go as $\sqrt{n}$. For each dangling bond, the weighted average (1 double and 2 single bonds per atom) of the binding energy for double and single

bonds will be used. This energy, using values from Adamson [21], is 3.6 eV. Therefore, for graphitic fragments,

$$\Delta G = n \cdot (8.14kT - 3.23) + 3.6\sqrt{n}.$$

Ion chromatography experiments [23, 24] reveal planar mono- and poly-cyclic rings as available isomers to C_n clusters. These ring structures seem to grow new "arms" at C_{10}-spaced intervals [23], i.e., mono-rings at C_{10}, di-rings at C_{20}, tri-rings at C_{30}, etc. The ring energies can be determined as linear energies plus an extra bond minus the bending strain energy. The average bending angle goes as n_b^{-1}, where n_b is the number of carbon atoms per ring. The number of rings per molecule goes as n_b, as mentioned above. Therefore, the strain energy is essentially constant in the two-dimensional structures. This gives

$$G_{n,ring} = G_{n+1,linear} - C.$$

Since

$$G_{10,ring} \approx G_{10,linear}, \tag{4.12}$$

[24, 31] then

$$C = G_{11,linear} - G_{10,linear}. \tag{4.13}$$

Note that odd and even differences need to be preserved, so, computationally,

$$G_{n,ring} = \frac{G_{n+2,linear} + G_{n,linear}}{2} + C.$$

Fullerenes with adjacent pentagons are less stable than those with entirely separated pentagons [18]. This "isolated pentagon rule" (IPR) has been justified by theoretical fullerene-isomer energy calculations [18]. An adjustment to the fullerene energies due to a cluster's failure to obey the IPR is, therefore, in order. This adjustment will stem from the notion that adjacent pentagons have a cost. Calculations have shown [20] the Gibbs free energy change for C_{60} with isolated pentagons going to C_{60} with two fused pentagon-pairs to be approximately 2.6 eV,

i.e., a cost of 1.3 eV per pentagon-pentagon adjacency. The number of adjacent pentagons for C_{20} is 30, while for C_{60} the number is zero. For simplicity, a linear increase in pentagon-pentagon adjacency from C_{60} to C_{30} is assumed, giving

$$\Delta GAdjust_{n,f}(n < 60) = 0.75(60 - n)1.3. \tag{4.14}$$

A further assumption of two adjacencies for $60 < n < 70$ will add 2.6 eV to these molecules' energy as well. The actual number of pentagon-pentagon abutments can differ significantly from these assumptions [18]. However, these will serve to show the effect of the adjacencies.

To recap, the Gibbs energies found above,

$$\begin{aligned}
\Delta G_{n,linear,even} &= (-7.9 + 7.2n)kT + (2.84 - 2.78n) \\
\Delta G_{n,linear,odd} &= (-7.9 + 7.2n)kT + (2.29 - 2.75n) \\
\Delta G_{n,ring,even} &= (6.5 + 7.2n)kT - (2.72 + 2.78n) \\
\Delta G_{n,ring,odd} &= (6.5 + 7.2n)kT - (3.21 + 2.75n) \\
\Delta G_{1,graphite} &= (8.14kT - 3.23) \\
\Delta G_{n,sheet} &= n \cdot (8.14kT - 3.23) + 3.6\sqrt{n} \\
\Delta G_{n,fullerene} &= n \cdot (8.14kT - 3.23) + \\
&\quad 25.2 + 7.32 \cdot ln(n/60) + \\
&\quad 0.975 \cdot (60 - n) \cdot \Theta(60 - n) + \\
&\quad 2.6 \cdot \Theta(n - 61) \cdot \Theta(69 - n),
\end{aligned} \tag{4.15}$$

where $\Theta(x)$ is zero for $x < 0$ and one, otherwise, provide us with the means to calculate the equilibrium partial pressure of each cluster, provided we have a set of stoichiometric equations defining the chemistry of the system.

4.3 The Par-Isomer model

Our first model, described by the set of equations defined by Eqn. 4.2,

$$nC_1(s) \rightarrow \frac{1}{4}C_{n,linear} + \frac{1}{4}C_{n,ring} + \frac{1}{4}C_{n,sheet} + \frac{1}{4}C_{n,fullerene}(= C_n),$$

will be referred to as the par-isomer model (PIM). Equilibrium cluster abundances for this model are shown in figures 4.21-4.27. Note the resemblance of Fig. 4.23 to the data shown in Fig. 4.19. The expected features are in evidence—the C_{60} dominance, the C_2 spacing, and the rapid decay in abundance to higher masses. The reduction of the C_{60} fraction with the increase of the higher-mass clusters is also supported by the empirical relations given in Eqns. 3.1.

It should be immediately evident that the C_2 spacing is not due to the fullerene or sheet isomer, but, instead, the result of basic differences in odd and even cluster behavior that led to their separate treatment in the linear and ring isomer energy calculations. If even and odd clusters were treated identically, the plot "envelope" would be maintained but odd clusters would be seen.

The abrupt cut-off of clusters below C_{60} is due entirely to the pentagon-pentagon penalty added to the fullerene energy. This is also true of the C_{62} through C_{68} cluster abundance reduction. Remember only a rough estimate of the actual number of adjacent pentagons for each cluster is represented here.

There are many useful predictions that can come from this analysis. For one, the chemical equation, 4.2, is one of carbon clusters in equilibrium with graphite. Therefore, graphite must be present for maximum fullerene production. This seems to be in conflict with the success of gas-phase fullerene production in benzene flames [4]. Perhaps the two techniques differ in their relative equilibrium, or the non-fullerene soot-particles present in both carbon-sublimation and benzene-flame techniques play a crucial role in these production systems.

Further, it is apparent that larger-fullerene production can be enhanced by increasing the temperature at the graphite—a result consistent with reports that large fullerene yield increases with increased power delivered to the graphite [14].

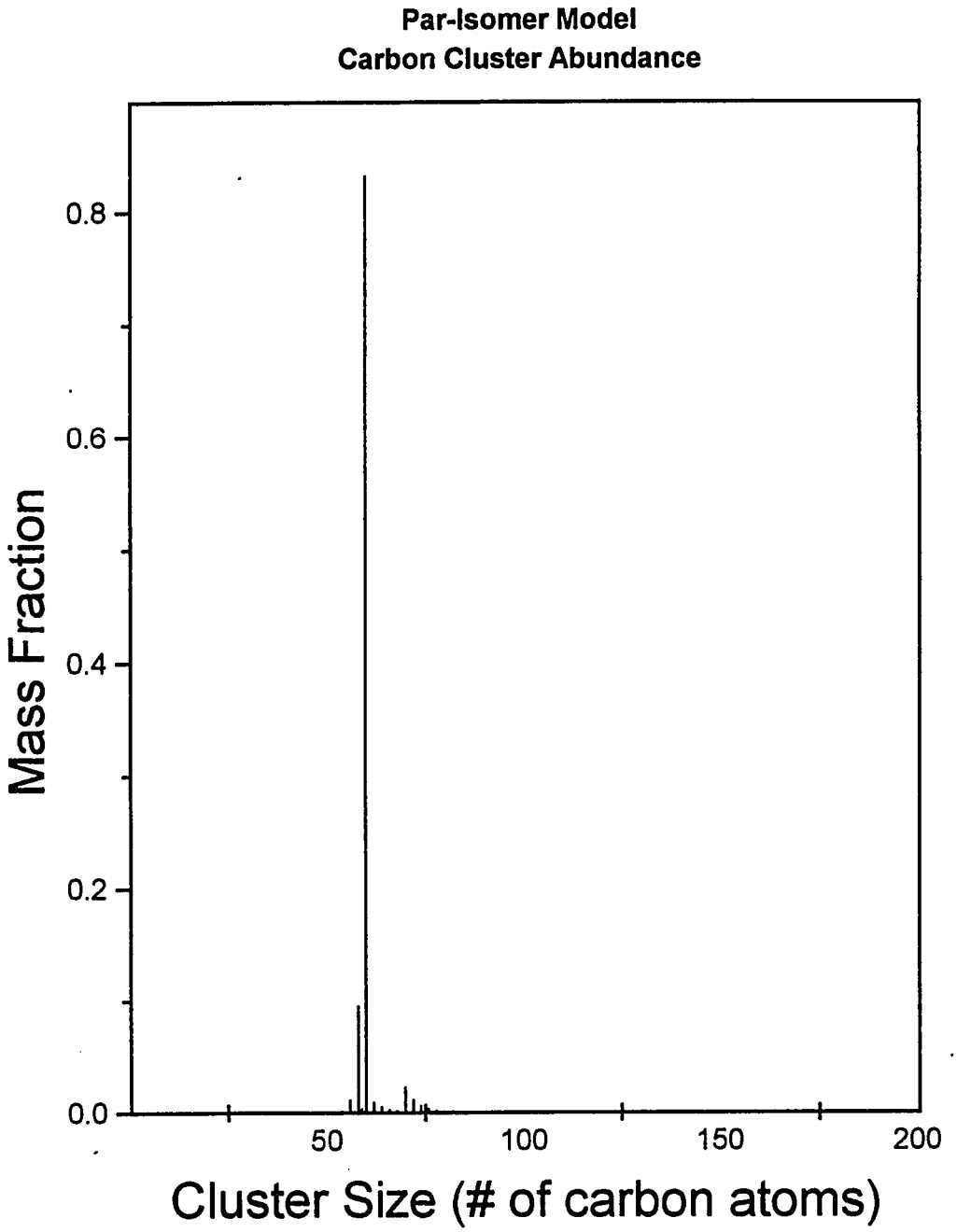

Figure 4.21: Par-Isomer model cluster-distribution at 4500 K.

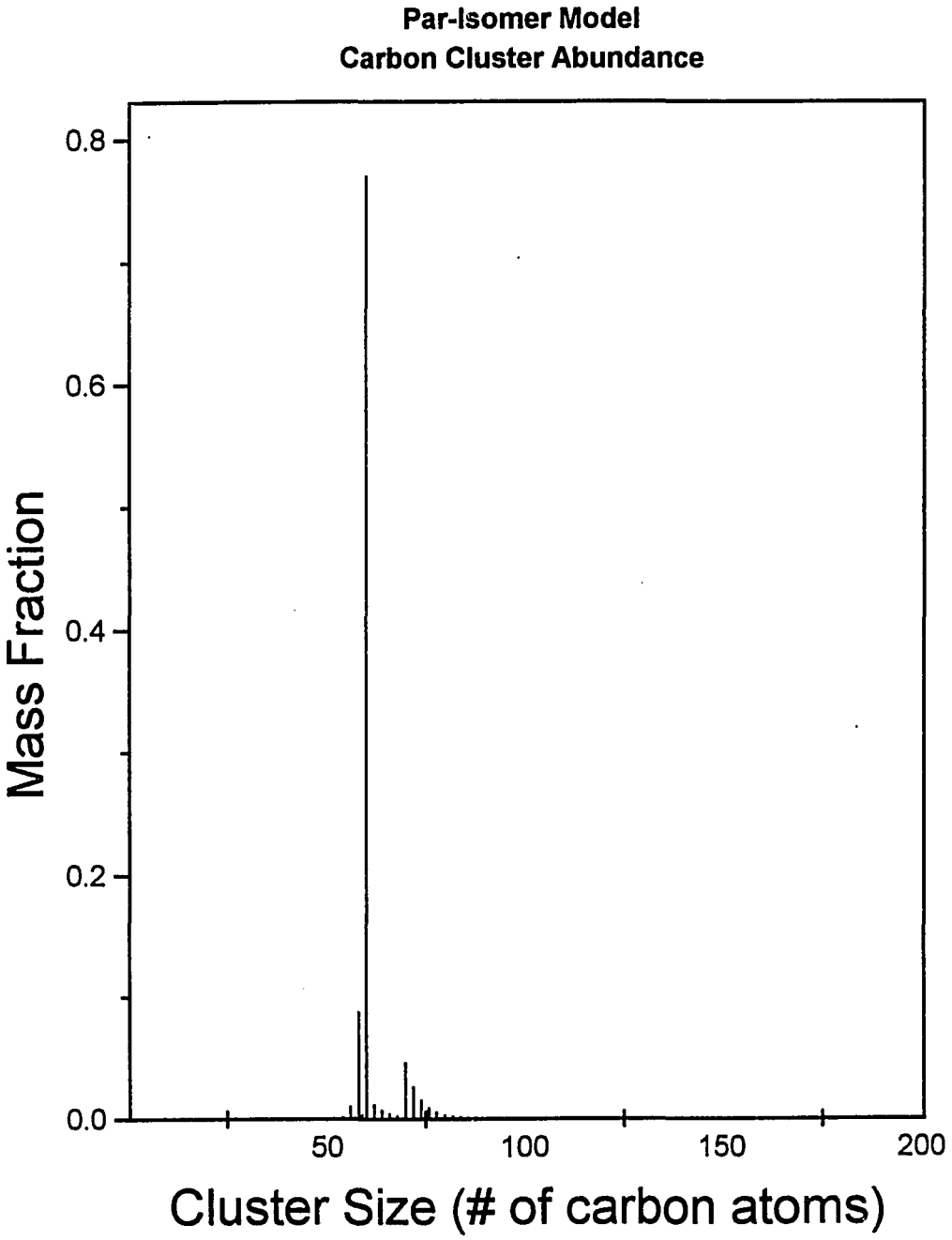

Figure 4.22: Par-Isomer model cluster-distribution at 4750 K.

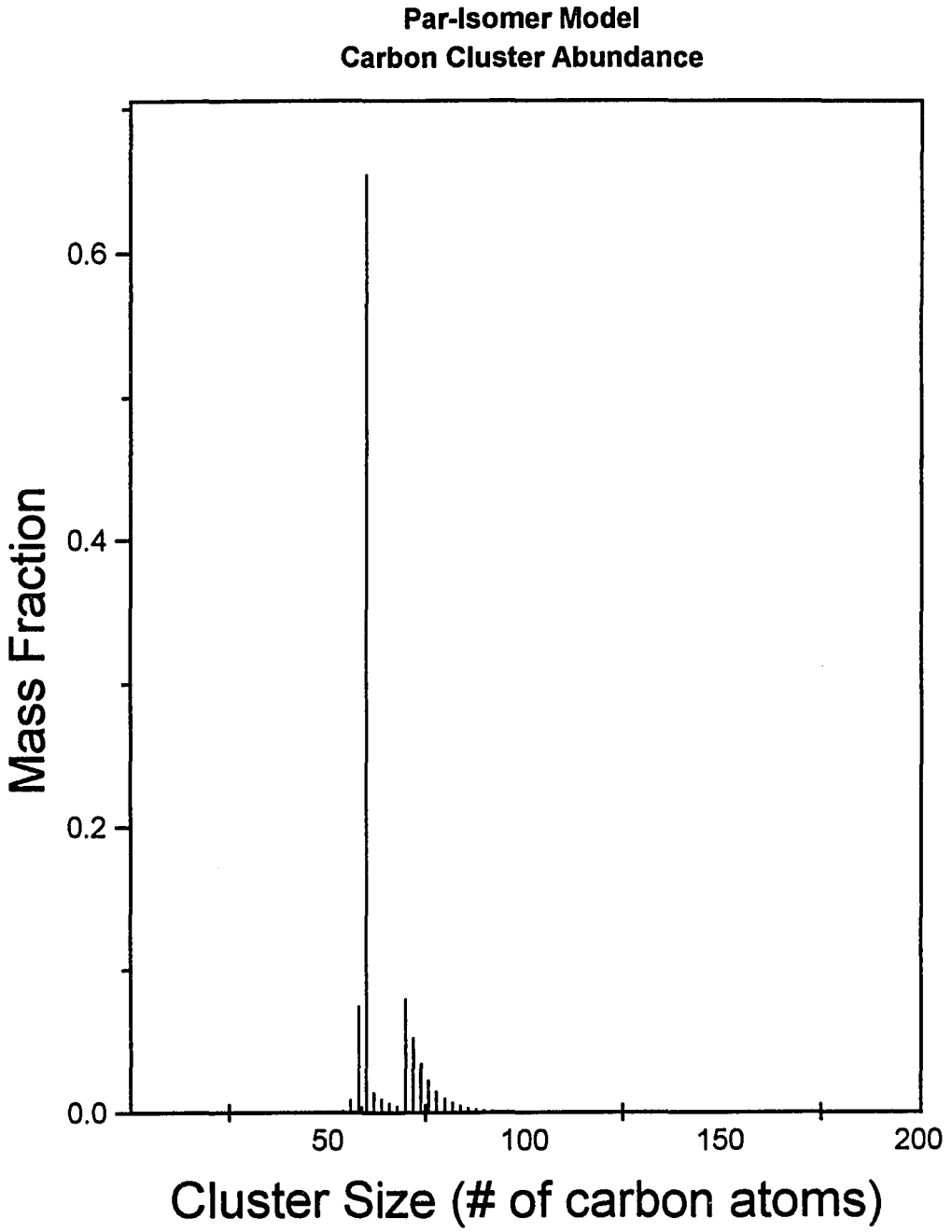

Figure 4.23: Par-Isomer model cluster-distribution at 5000 K.

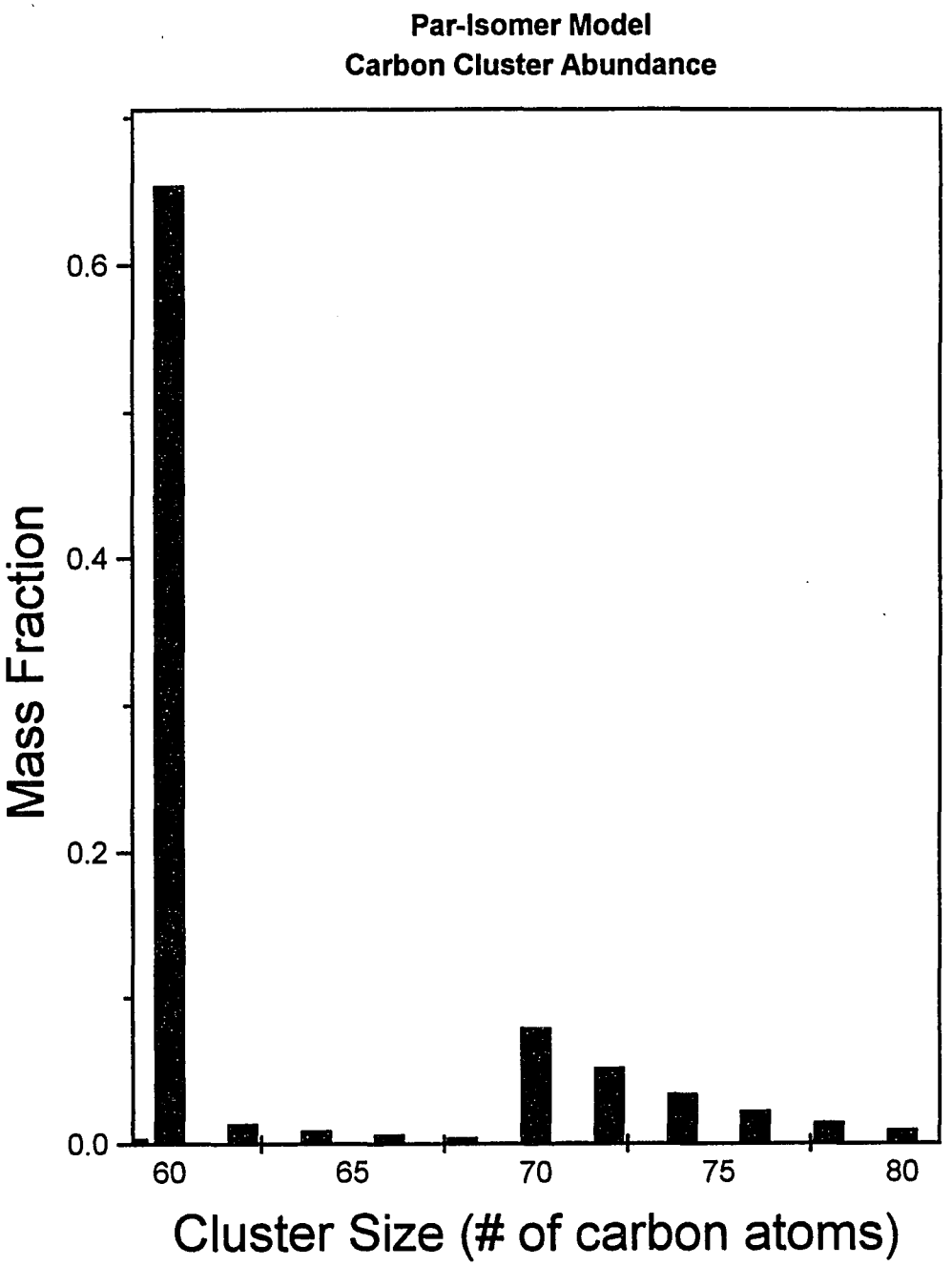

Figure 4.24: Par-Isomer model cluster-distribution at 5000 K. Note the C_2 spacing.

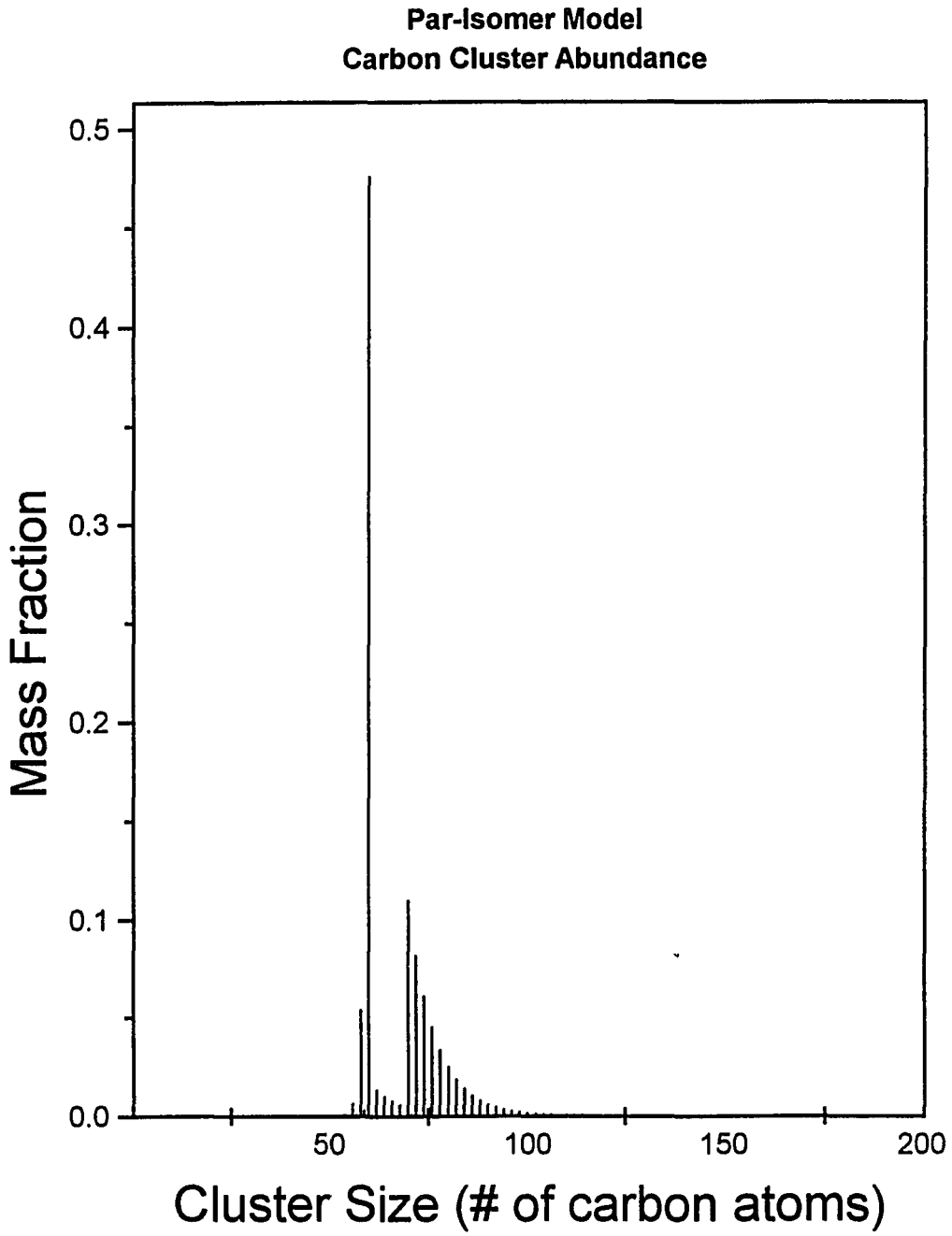

Figure 4.25: Par-Isomer model cluster-distribution at 5250 K.

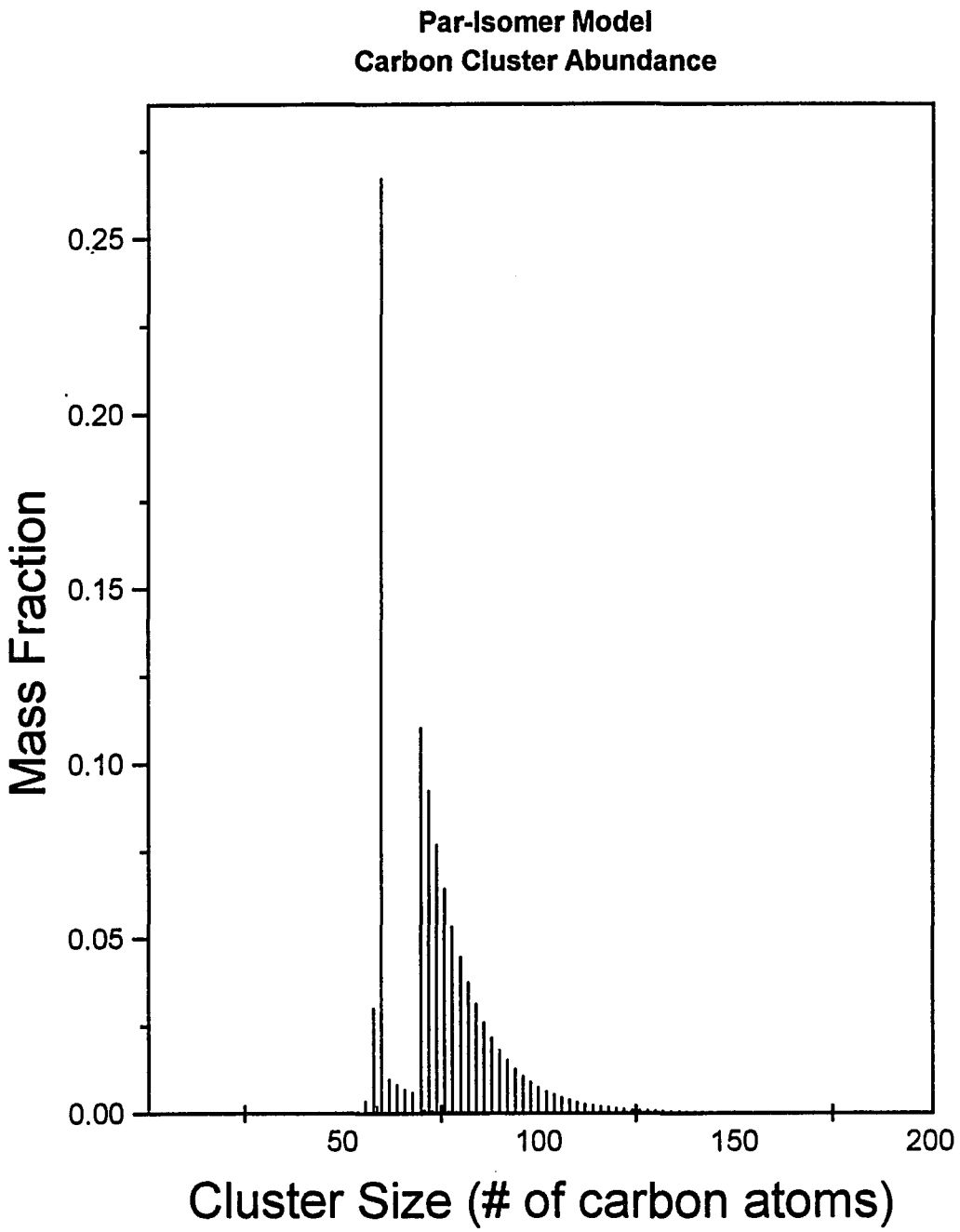

Figure 4.26: Par-Isomer model cluster-distribution at 5500 K.

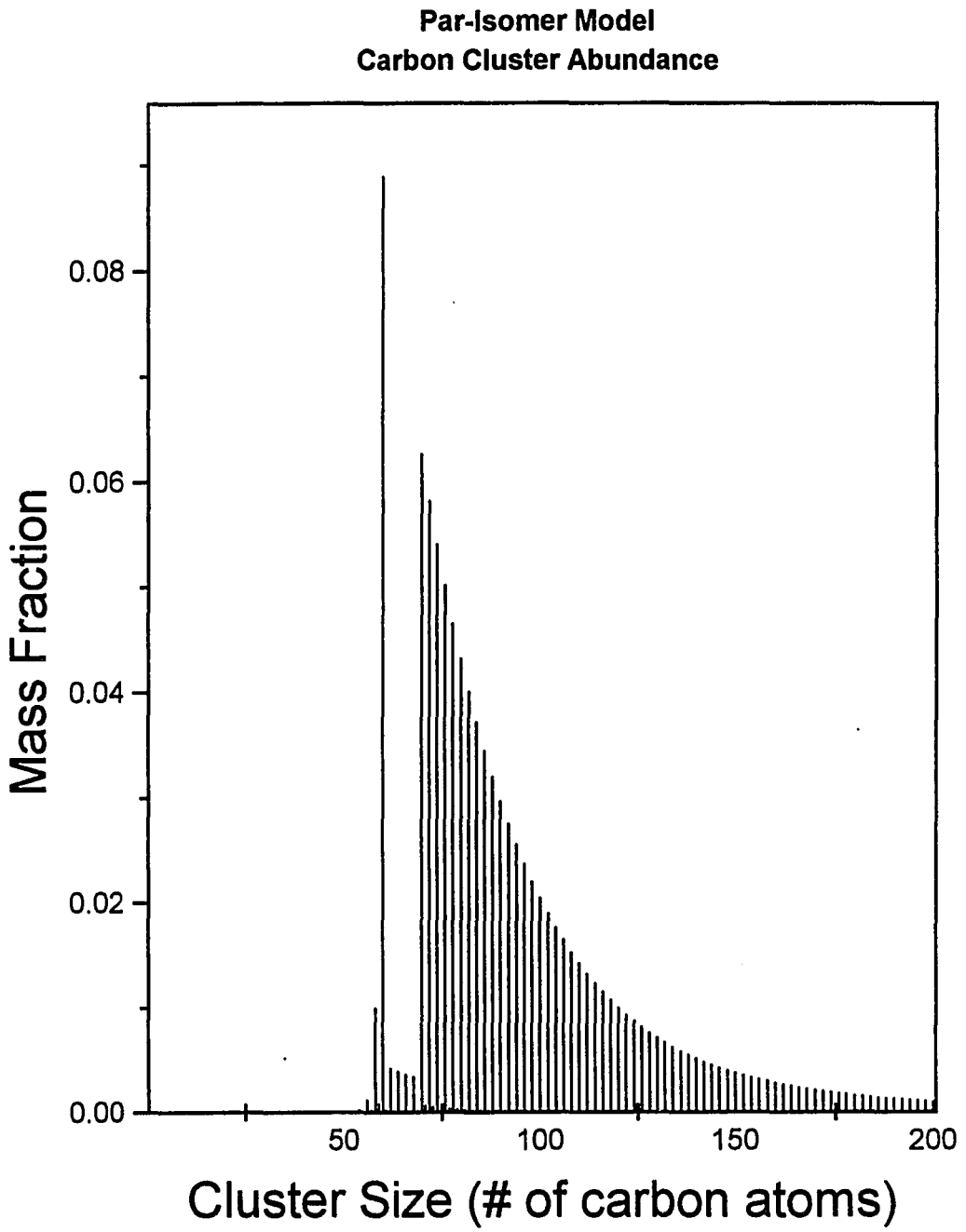

Figure 4.27: Par-Isomer model cluster-distribution at 5750 K.

An open question is how this analysis explains fullerene-production pressure-dependence. It is common knowledge that fullerene production has a maximum-yield pressure, although its value seems chamber dependent [14]. A possible explanation is that, as the clusters diffuse from the graphite to the chamber wall, the cluster-cluster reactions are no longer moderated by the graphite.

Although the calculations above show a positive relationship to experimental data, there are some issues not yet resolved. In the analysis, fullerene isomers for $C_{n<20}$ have been allowed in spite of being geometrically impossible. The same is true for ring structures below $n = 3$. If the calculations are modified to fix this oversight, the small-cluster dominance referred to by Slanina, et al. [17], reappears. The local relative abundances in the mass region around C_{60} remain as shown, but the partial pressures are minuscule.

4.4 Selected cluster behavior in the PIM

The relationships discovered in the experiment section, given in equations 3.1, prompt us to test how well theory reproduces this behavior. Figure 4.28 shows the temperature dependence of the abundances of C_{60}, C_{70}, C_{76}, C_{78}, and C_{84} in the PIM. Figure 4.29 expands on this by showing how the last four of this set vary with the fractional abundance of C_{60}. Finally, figure 4.30 shows the total selected fullerene yield versus the C_{60} yield. This provides a direct comparison of PIM with the empirical results.

The gross behavior shown in figure 4.29 mirrors that found in Figs. 3.15-3.18. The larger clusters decrease in fractional abundance with an increase in C_{60} fraction. The relationships are monotonic and gentle with C_{76} and C_{78} being markedly linear. The PIM-based total yield versus C_{60} yield shown in figure 4.30 has a linear character like that found in the experimental section.

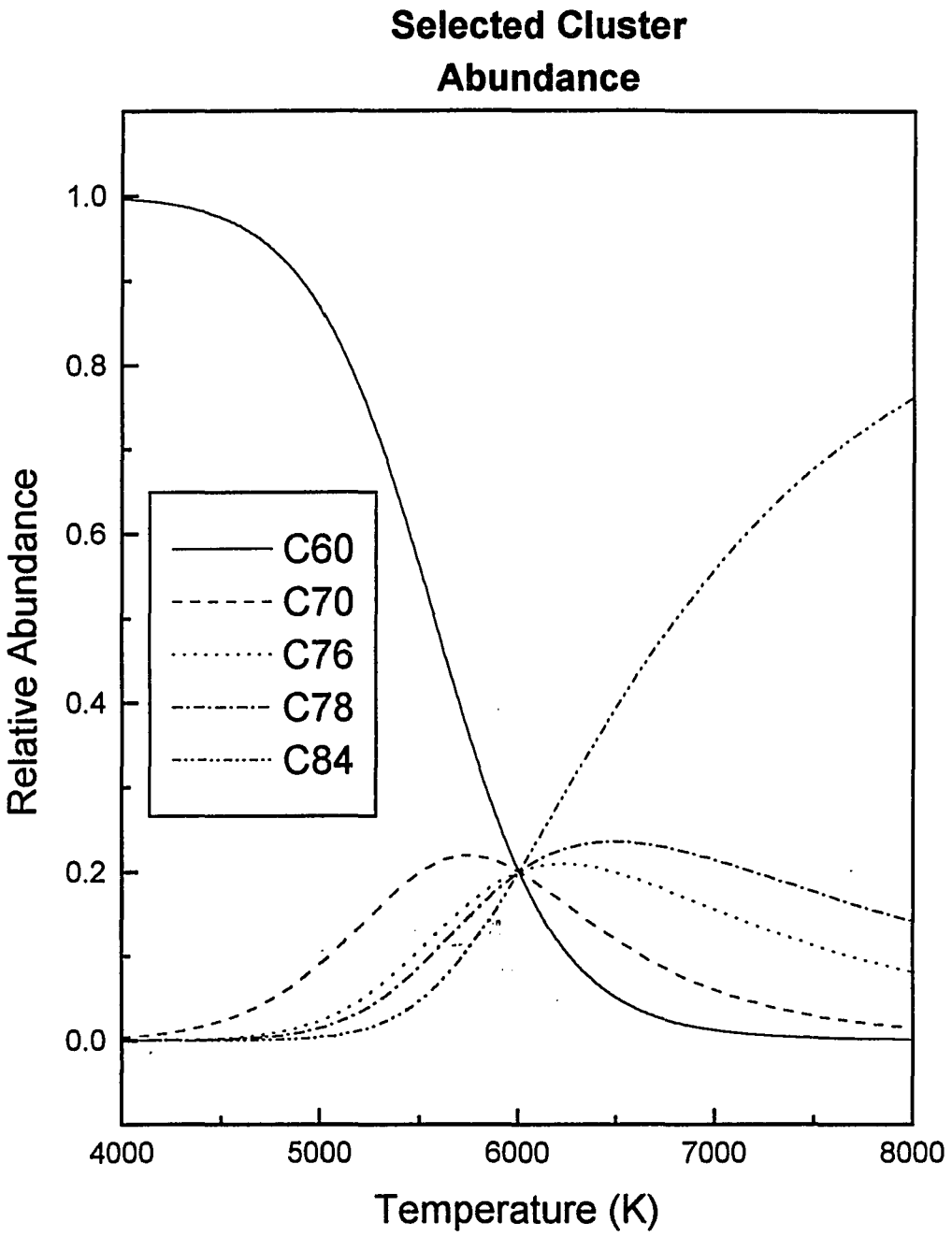

Figure 4.28: Par-Isomer model selected cluster-distribution.

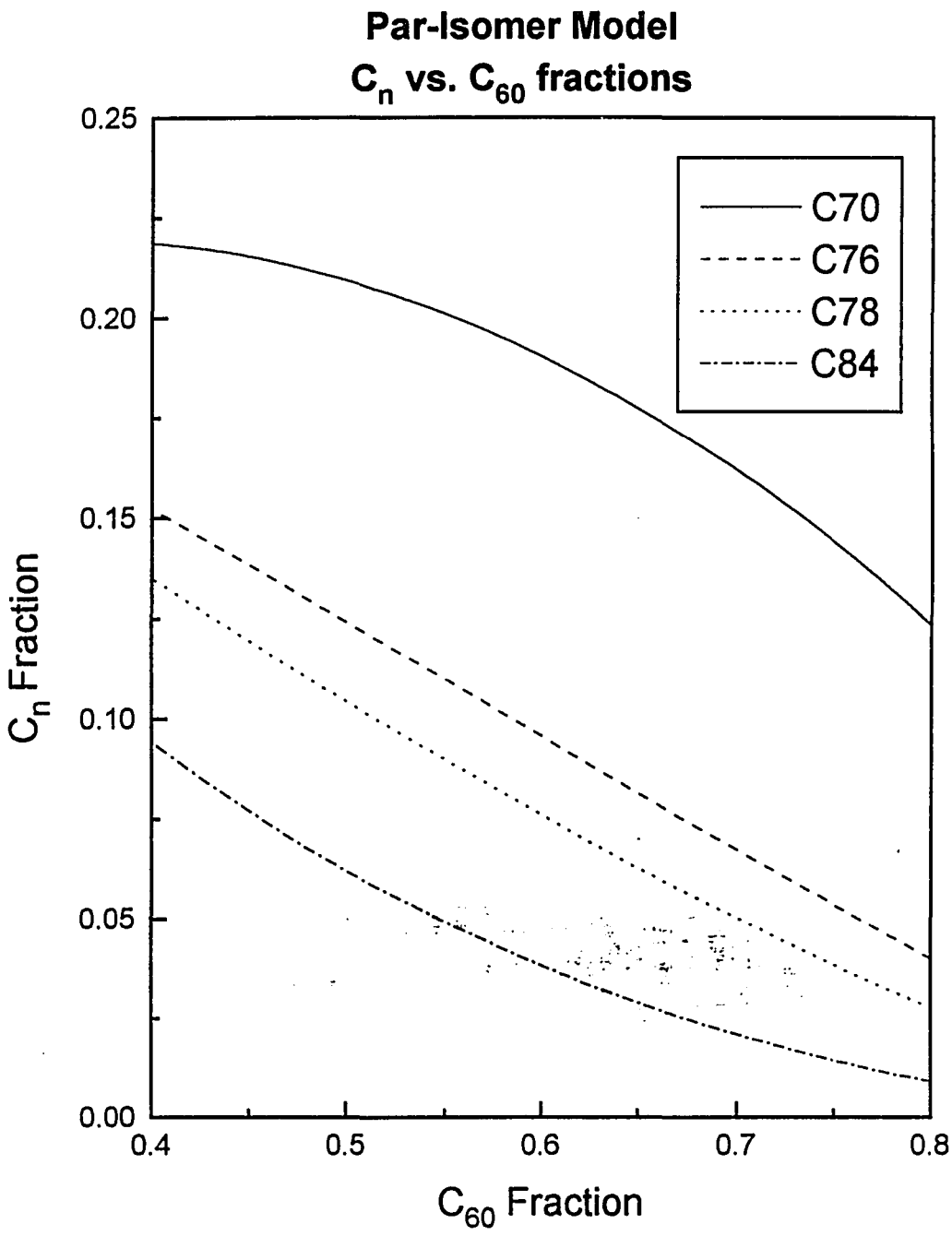

Figure 4.29: Par-Isomer model fractional abundance relationships.

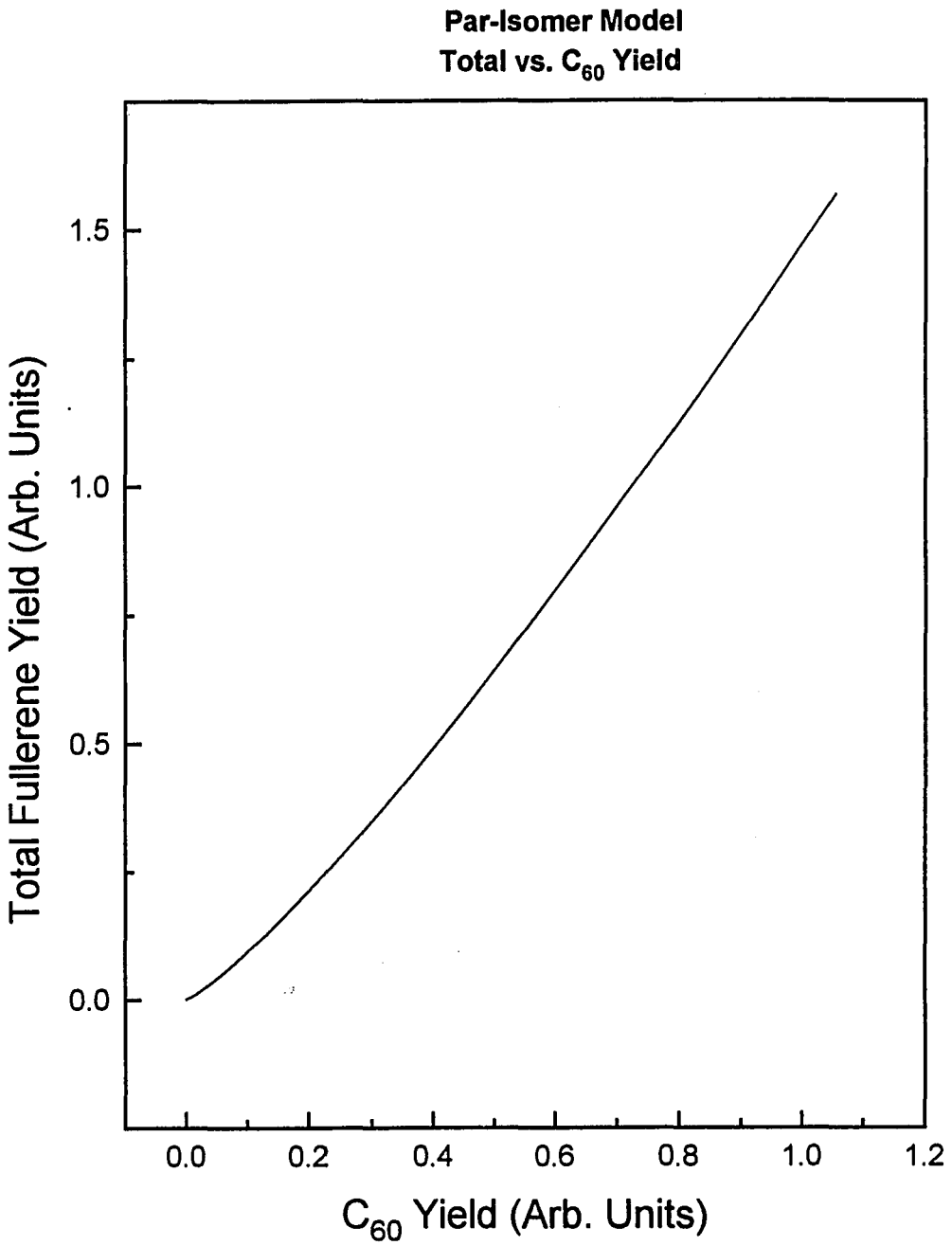

Figure 4.30: Par-Isomer model fractional abundance relationships.

4.5 The Biased-Isomer model

If, instead of using the relationships given in Eqn. 4.2, we used the larger set

$$nC_1(s) \rightarrow C_{n,\alpha}, \tag{4.16}$$

where α labels the cluster isomer, then the cluster-mass distribution would be like that shown in Fig. 4.31. This model will be known as the biased-isomer model (BIM). The small-cluster dominance in this view differs from what one would expect based on fullerene abundances. However, if the temperature is adjusted upward, we find that a distribution peaked at around C_{60} obtains at 5325 K (see Fig. 4.32). The close-up view around C_{60} in Fig. 4.34 shows the even-cluster dominance as before, but the $C_{n<60}$ and C_{62} to C_{68} clusters are now quite evident. It is important to note that the clusters shown in Figs. 4.32, 4.33, and 4.34 are almost exclusively linear chains and rings. One should also note the natural reproduction of the two distinct mass-spectral regions found in Fig. 1.1.

Although BIM provides a carbon-cluster distribution satisfying many of the experimental observations, it does not reproduce the C_{60} dominance and relative fullerene abundances as well as PIM. An obvious reason for the failure is that the fullerene isomers are many orders of magnitude less abundant in BIM than the ring and linear isomers at the temperatures shown. At high temperatures near graphite, PIM focuses on fullerene isomers and BIM stresses the ring- and linear-isomer abundances. BIM is far more realistic in this regard.

4.6 Isomer abundances

Since the peaked distribution provided by BIM is one of linear chains and rings, the annealing behavior of these isomers into fullerenes becomes important to the model. Using the Gibbs energies found above and the stoichiometric relations

$$C_{n,\alpha} \rightarrow C_{n,\beta},$$

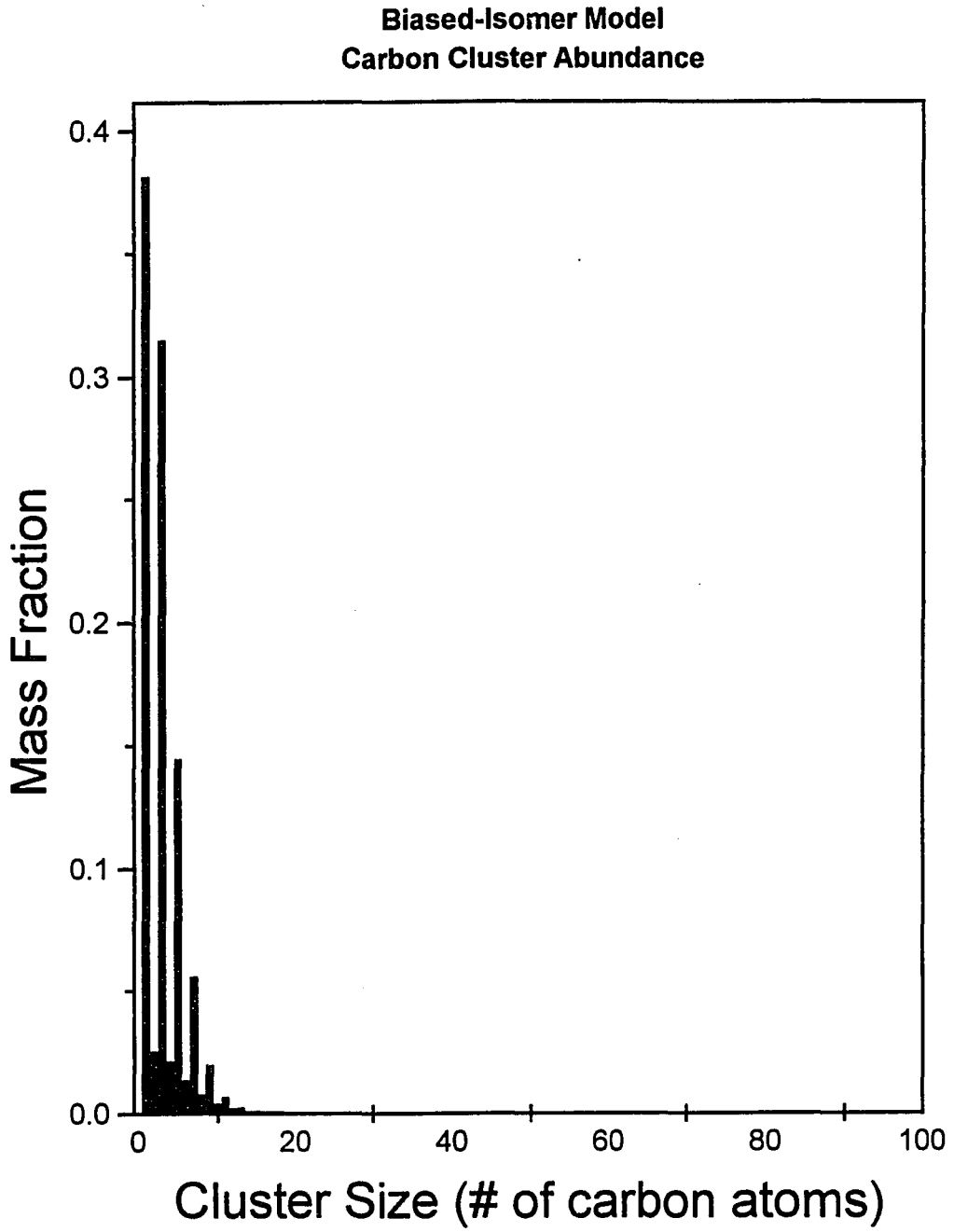

Figure 4.31: Biased-Isomer model cluster-distribution at 4500 K.

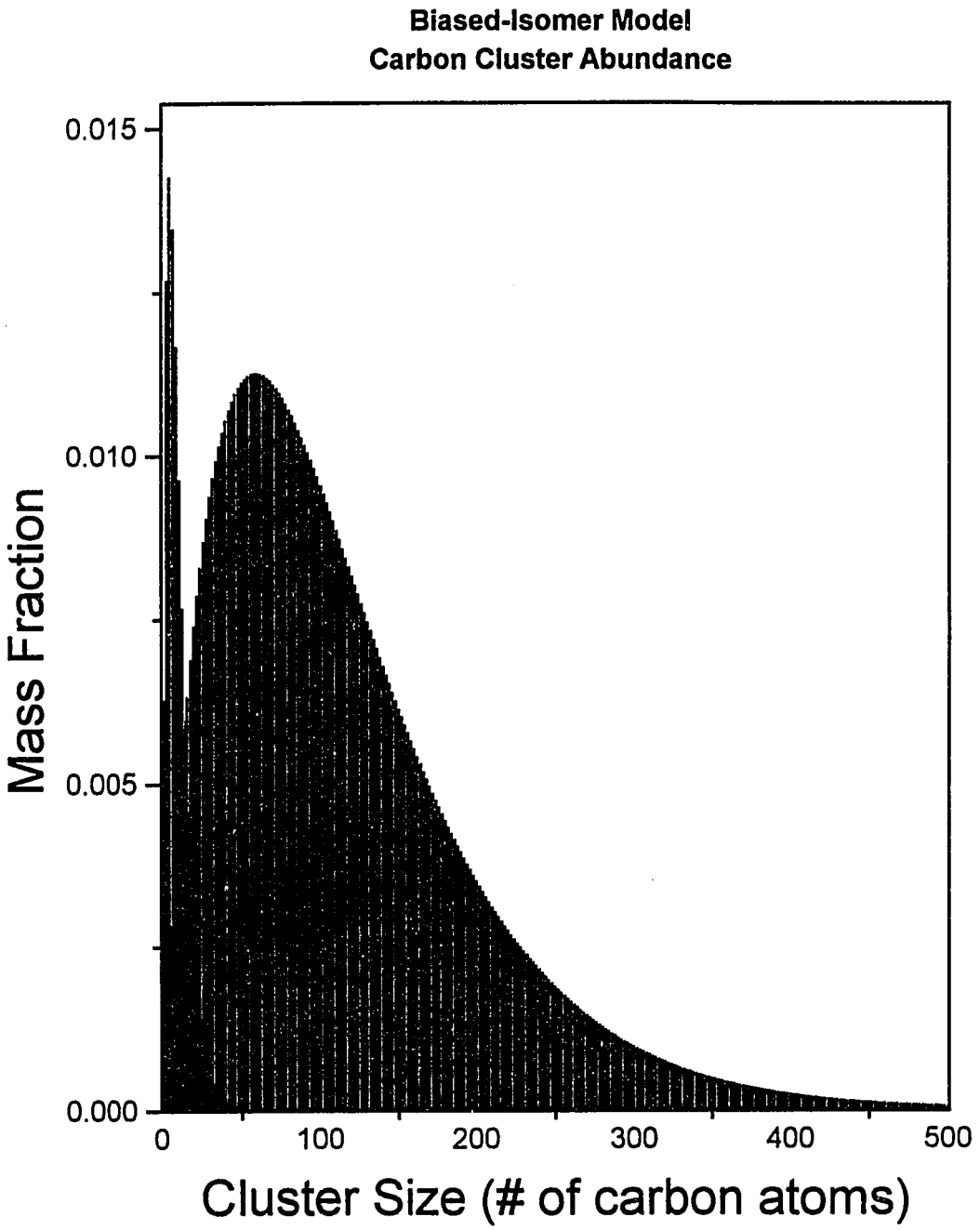

Figure 4.32: Biased-Isomer model cluster-distribution at 5325 K.

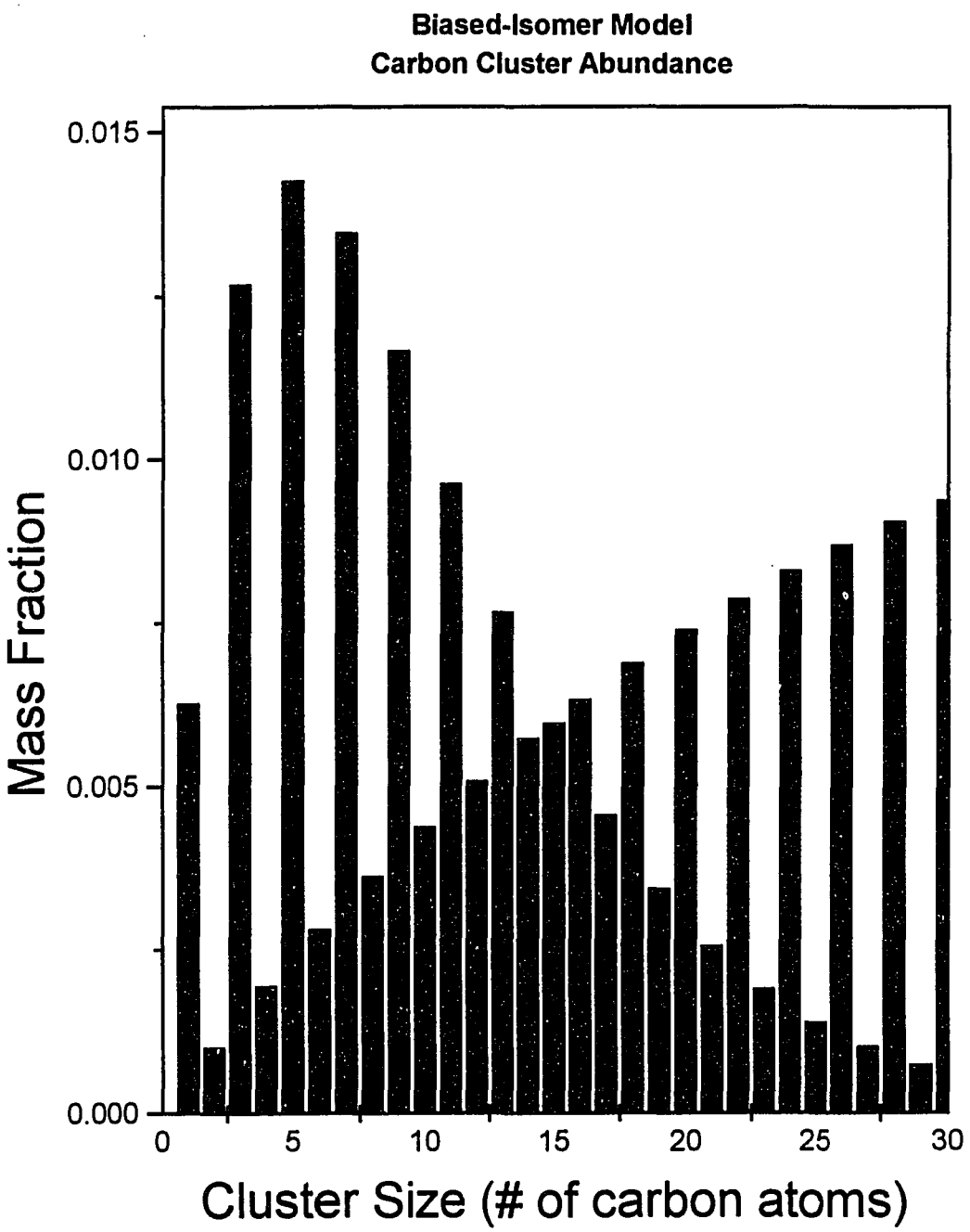

Figure 4.33: Biased-Isomer model cluster-distribution at 5325 K. Note C_1 spacing at low n giving way to C_2 spacing as n increases.

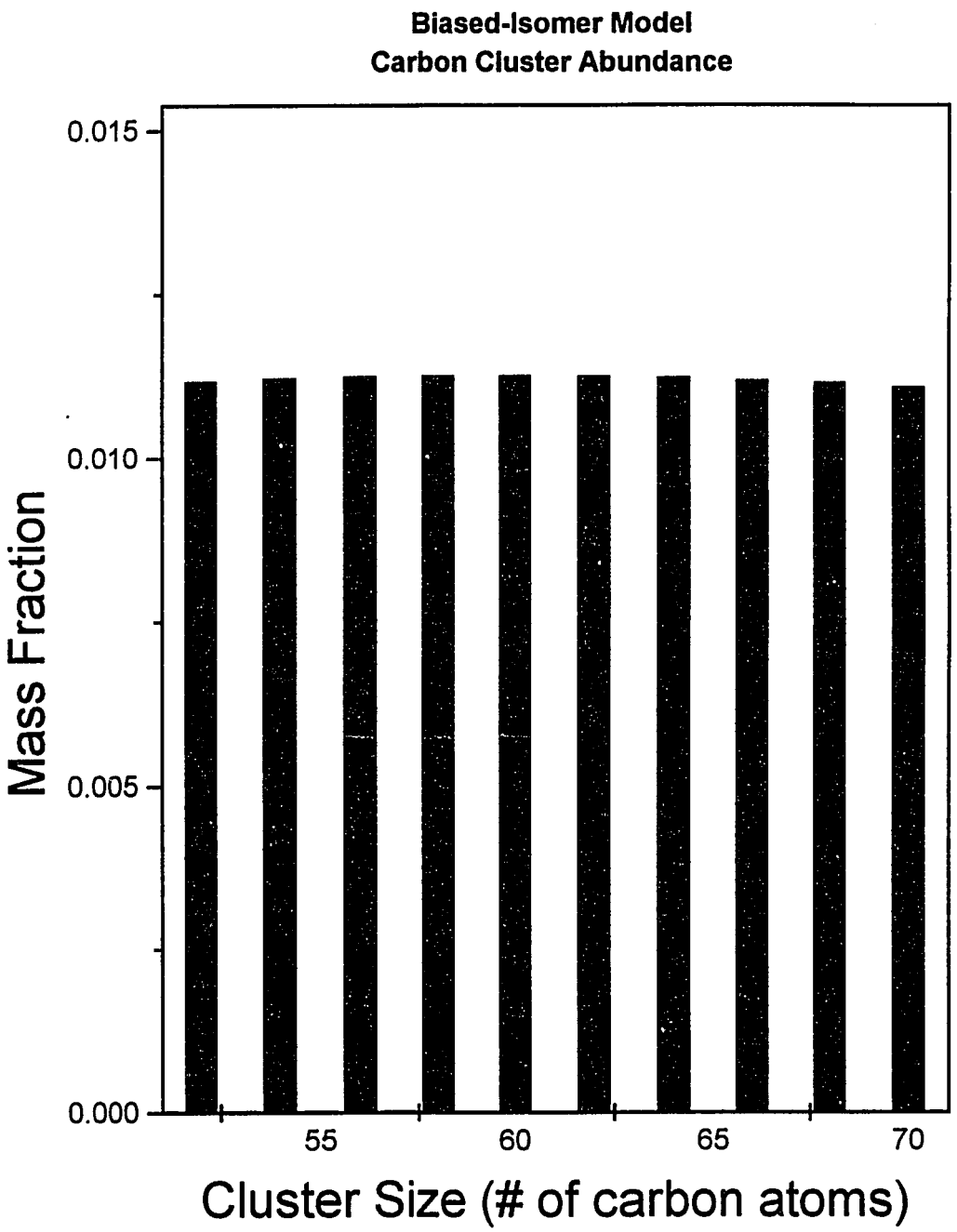

Figure 4.34: Biased-Isomer model cluster-distribution at 5325 K. Note C_2 spacing is now completely dominant.

where α and β label isomers of the n-atom carbon cluster, one can determine the equilibrium relative abundances of the various isomers. Figures 4.35-4.37 show the relative abundance of linear chains, rings, fullerenes, and graphite-like fragments at temperature ranging from 300 to 6000 K.

In the BIM view, the cluster-size distribution is dictated by a state of equilibrium at the graphite. The clusters then diffuse toward the cooler regions of the chamber, annealing into the favored fullerene isomers as they go. The effect of cluster-cluster chemistry during diffusion, however, is unknown and might be significant.

4.7 Common model features

As mentioned above, one cannot write down a "wrong" stoichiometric equation unless it does not balance. Both Eqns. 4.2 and 4.16 are equally correct. However, it is possible that either, or both, may never be realized in the fullerene synthesis reactions. What these two models show, is that equilibrium analysis of the fullerene-production environment can give results that reflect the trends and qualitative features found in experiment. Since both rely on the presence of graphite to achieve a distribution peak, it is likely that any equilibrium description will require this presence. In addition, the C_2 spacing found for the higher-mass clusters, being a feature of the odd-even cluster differences, should be common to all of the equilibrium models.

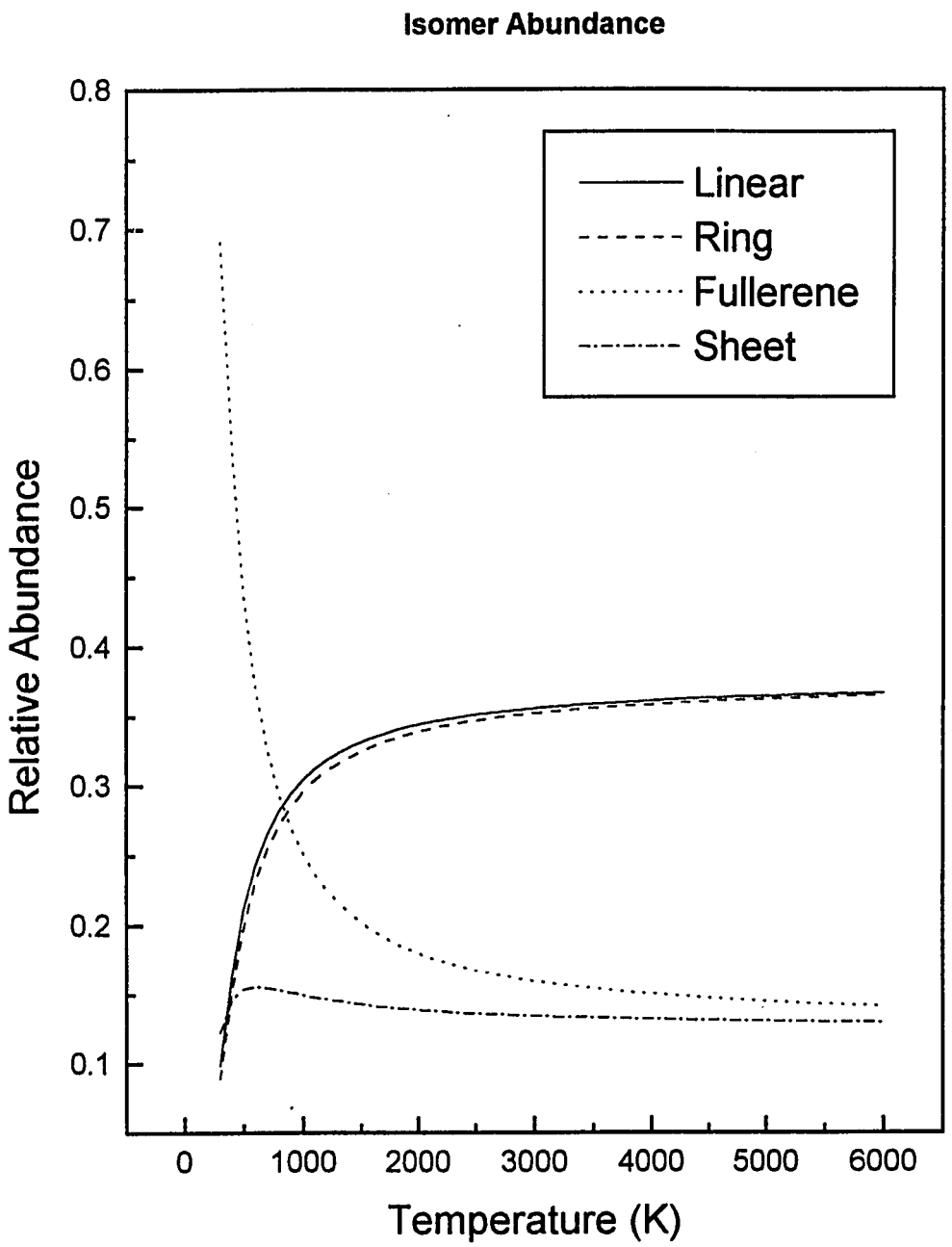

Figure 4.35: Isomer abundance for C_{60}.

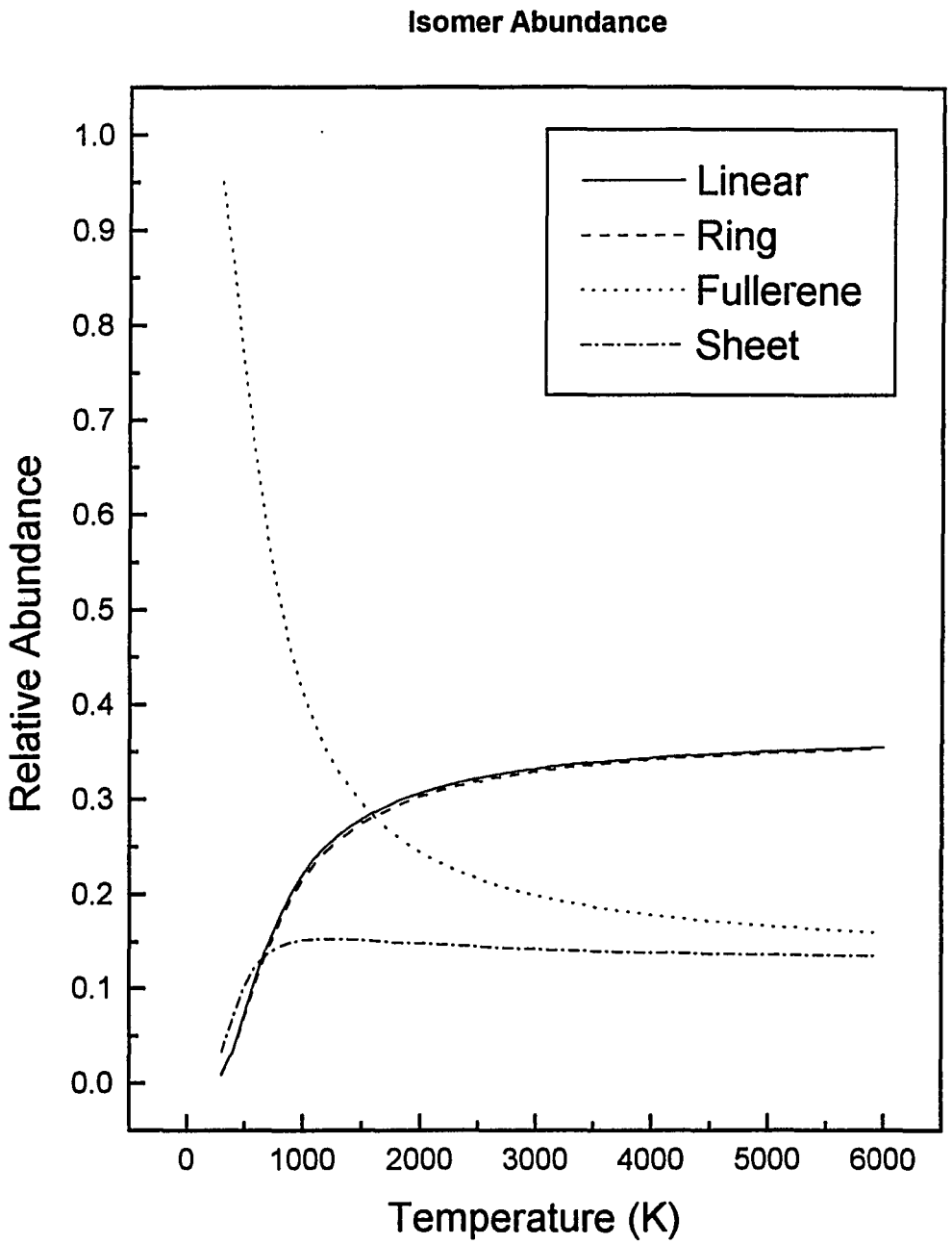

Figure 4.36: Isomer abundance for C_{70}.

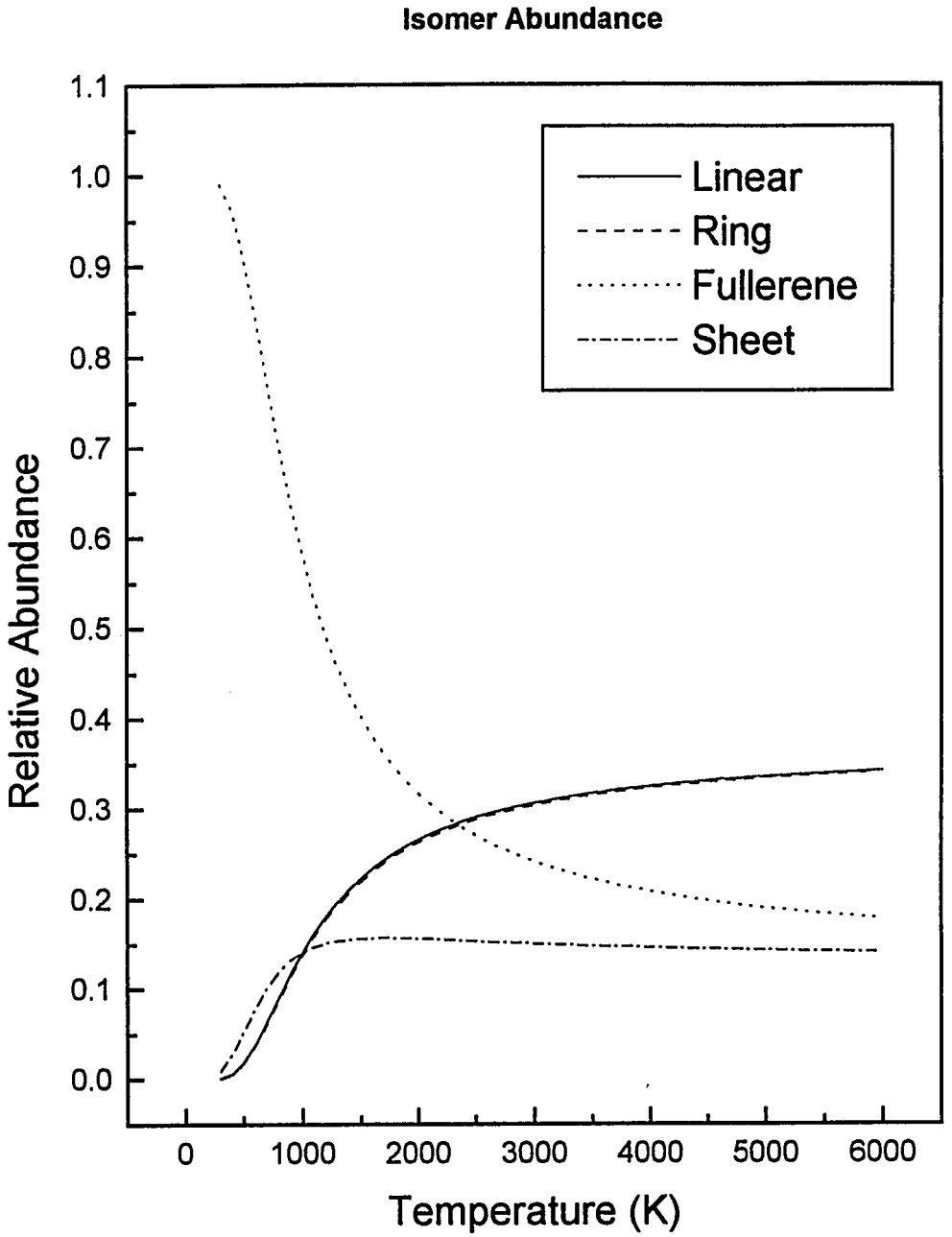

Figure 4.37: Isomer abundance for C_{84}.

CHAPTER 5

CONCLUSIONS

The experimental work in this effort shows a predictive linear relationship among the fullerene species produced in carbon-evaporation production. These relationships have not been previously reported and seem to indicate that an equilibrium description of fullerene production is valid.

The theoretical work herein also finds that an equilibrium description of fullerene production may be possible. The models offered in support of an equilibrium description reproduce many essential features of fullerene mass spectra and the relative C_n yield variations seen in experiment. The stoichiometric equation chosen to represent the clustering chemistry in the chamber dictates the results of these equilibrium calculations. Common to the equilibrium views explored, however, are

- a solid graphite phase in the system is essential to achieve a peaked cluster-distribution,
- the C_2 spacing at larger cluster sizes and the C_1 spacing at smaller sizes is due to an essential difference between odd and even clusters and not caused by a fullerene effect, and
- the peaked distribution afforded by the presence of graphite and the odd/even cluster differences combine at some value of the temperature to produce two, seemingly separate, distributions—one at high mass numbers the other at low numbers with C_{30} marking the territory in between.

In both the experimental and theoretical areas, further work is needed. Experimentally, turbulence patterns and their effect on fullerene yield need to be investigated. Also, the linear relationships need to be compared to other fullerene-production-chamber results. Theoretically, cluster equilibrium with graphite needs to be pursued further with transport processes included in the relevant calculations.

APPENDIX A

UV-Visible Absorption Analysis

Normal, as opposed to nonlinear, optical-absorption measurements are accomplished by measuring the unimpeded light intensity at some wavelength, and then the intensity at the same wavelength with a sample inserted into the beam. The transmission factor is determined using

$$T = \frac{I}{I_0},$$

where I and I_0 are the intensities with and without the sample in the beam, respectively. The extinction of the light as it progresses through the sample is well described as an exponential decay with transit distance, x:

$$I = I_0 \exp(-\alpha \cdot x),$$

where α is known as the extinction coefficient. This is known as Bouger's law. It is equivalently stated in terms of the optical density OD of a substance

$$I = I_0 10^{(-OD \cdot x)},$$

with the usual relationships between the associated common and natural logarithms.

Either OD or α can be expressed in terms of the molar concentration of a solution, the expression being proportional to the concentration in both cases. This means that dividing OD or α by the concentration for a known sample gives a technique to measure the concentration of an unknown sample by measuring its absorption spectrum.

For multiple-component solutions, the optical density is proportional to a weighted sum of the concentrations. Therefore, determination of each concentration in a multicomponent solution requires at least as many absorption measurements as unknowns in the solution—the resulting set of linear equations are solved using whatever numerical technique is preferred.

One necessary condition for a reliable inversion is the linear independence of the pure component spectra. That is, if any of the components' spectrum is a linear combination of the other spectra, the inversion will be singular. In practice, linear dependence is a matter of degree. Inversion will be possible, but highly unreliable, if the spectra are not independent "enough". Determination of a system's linear independence, and the solution to the inversion problem at hand, can be facilititated by a technique known as singular-value decomposition [37].

Singular-value decomposition (SVD) is a technique where a matrix, **M**, is decomposed into the product of a column orthonormal matrix, **U**, a diagonal matrix, **w**, and an orthonormal square matrix, **V**, i.e.,

$$\mathbf{M} = \mathbf{U} \cdot \mathbf{w} \cdot \mathbf{V}. \tag{A.17}$$

M need not be square for this decomposition. The matrices, **U**, **w**, and **V** found by this technique have a direct bearing on the problem at hand. The columns of **U** are an orthonormal set of vectors spanning the space defined by the columns of **M**. The elements of the diagonal matrix, **w**, give the eigenvalues of the decomposition; their relative magnitudes give one a measure of how important each basis vector (columns of **U**) is in the system. If one performs SVD on an n x p matrix ($n > p$) and finds that the p x p matrix, **w**, contains m insignificant elements, as compared with the other $p - m$ elements, the actual number of independent dimensions, i.e., number of linearly independent columns in **M**, is given as $p - m$. This is how we will analyze our spectra below for how invertible our problem is.

Equation A.17 also shows how one solves a linear equation using SVD. Since **U** and **V** are column orthonormal their inverses are their transforms. The

inverse of $\mathbf{w}$ is simply the inverse of its elements. Therefore,

$$\mathbf{M}^{-1} = \mathbf{V}^T \cdot \mathbf{w}^{-1} \cdot \mathbf{U}^T.$$

By setting the elements of $\mathbf{w}^{-1}$ corresponding to insignificant values of $\mathbf{w}$ to zero, we remove them from the inverse problem and get a more reliable value for the vector solution. A more complete discussion of SVD and the implementation used herein can be found in reference [37].

Separation of the fullerenes can be accomplished, to some extent, using column and high-performance-liquid chromatography techniques. Using column chromatography, samples of pure C_{60} and C_{70} were obtained in our lab. These samples were weighed and UV-Visible absorption measurements taken using a Cary 118 spectrophotometer at 1 nm spacings from 350 nm to 800 nm. These absorption spectra were concentration-normalized by dividing the optical density given by the spectrometer for each wavelength by the molar concentration of the sample. The resultant concentration normalized spectra are shown in Figs. A.38 and A.39.

C_{76}, C_{78}, and C_{84} absorption spectra were taken from the work of Diederich, et al. [34, 35, 36]. The C_{84} spectrum was not accompanied with absolute absorption values, so the raw data were adjusted by a factor to give an absorption at 400 nm near that of the other constituents—an ad-hoc normalization procedure.

After constructing the columns of a matrix from the pure spectra, SVD was performed and the following set of eigenvalues (diagonal constituents of $\mathbf{w}$) were found:

$$w_{i,i} = 992.5, 236.9, 107.2, 27.8, 62.6.$$

The usual criteria used to define "insignificant" in SVD analysis is that a value be 6 orders of magnitude smaller than the largest $\mathbf{w}$ value. None of these values meet that criterion, so the set of absorption spectra are assumed linearly independent "enough" and all constituents determinable.

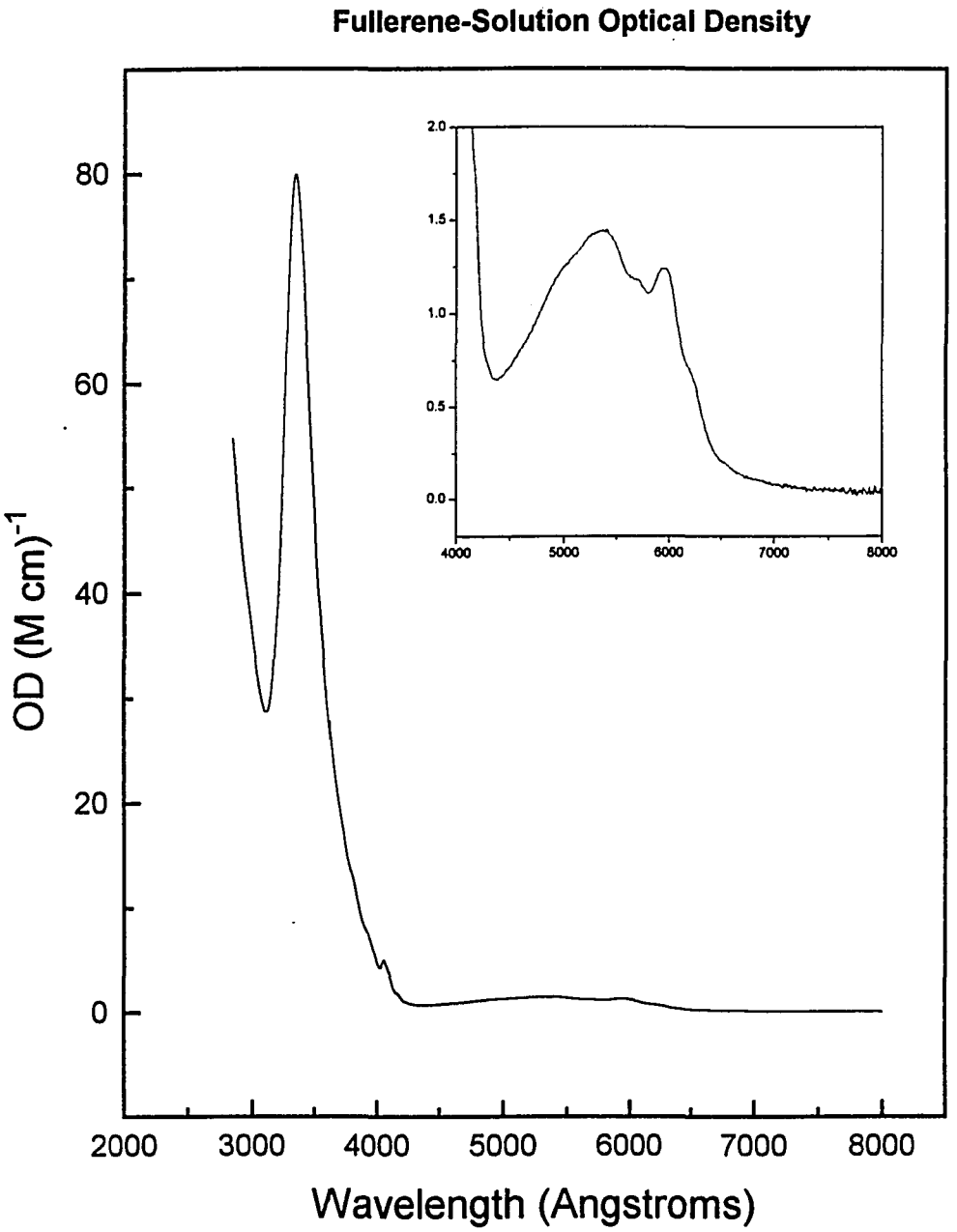

Figure A.38: Molar concentration-normalized C_{60} UV-Visible absorption spectrum.

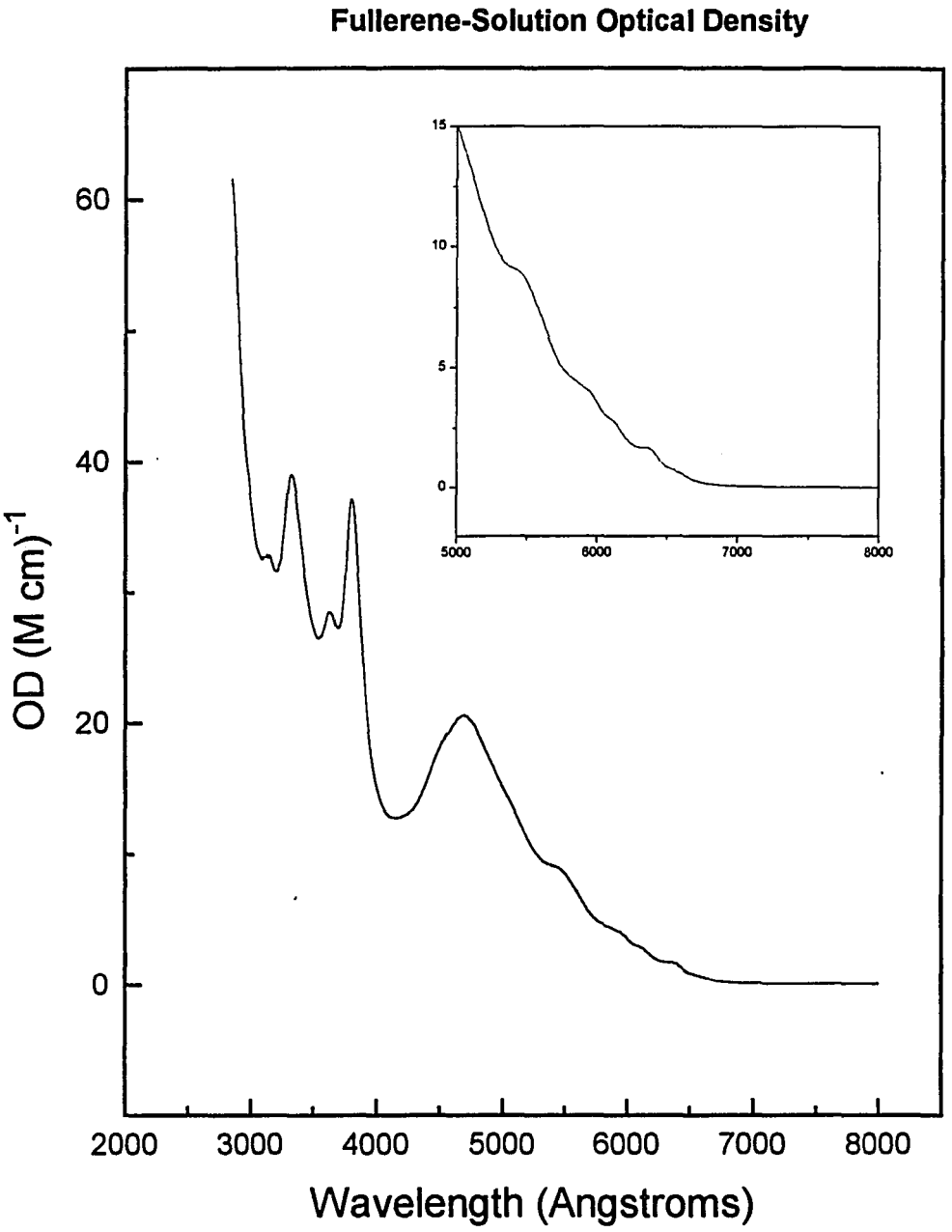

Figure A.39: Molar concentration-normalized C_{70} UV-Visible absorption spectrum.

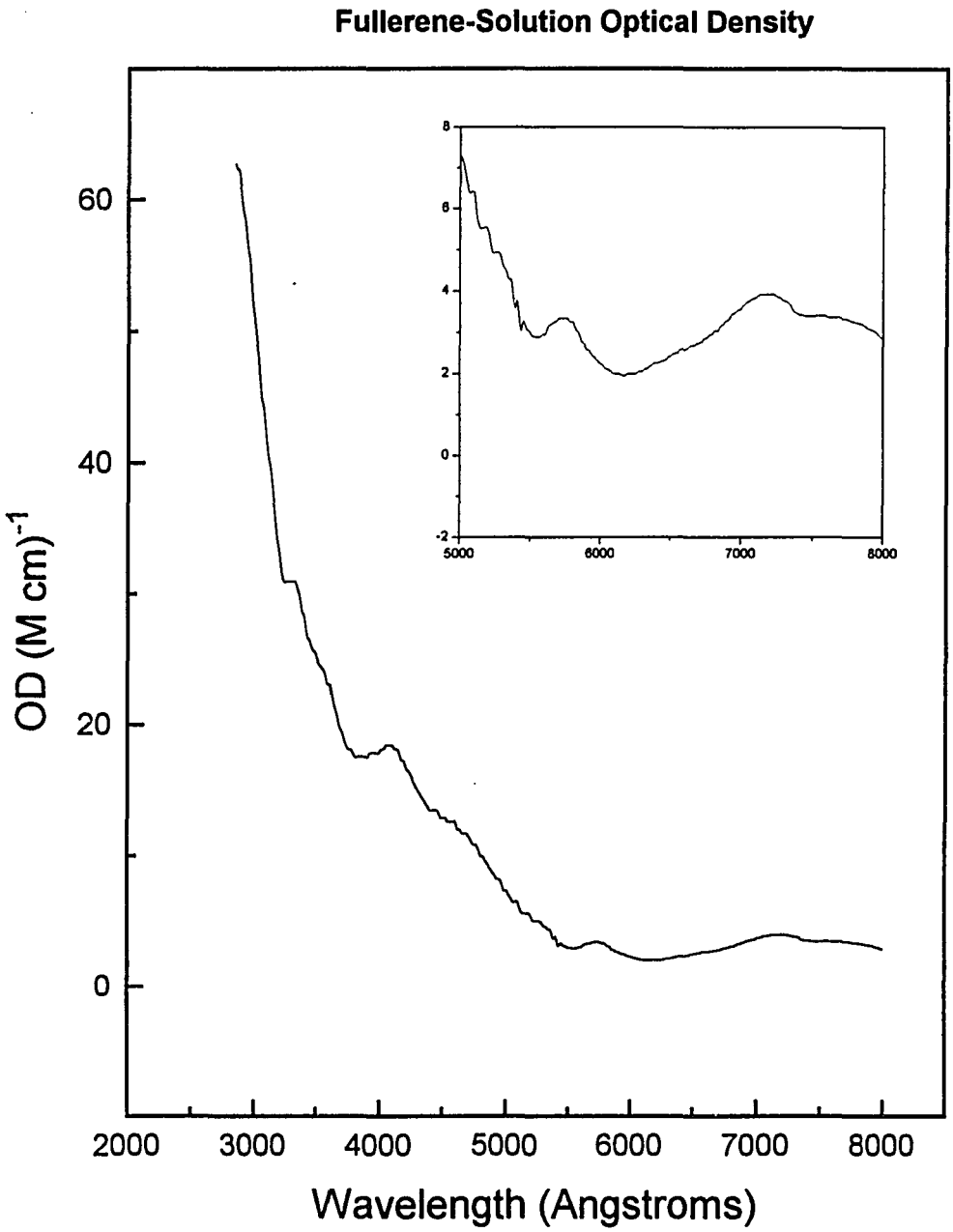

Figure A.40: Molar concentration-normalized C_{76} UV-Visible absorption spectrum from reference [34].

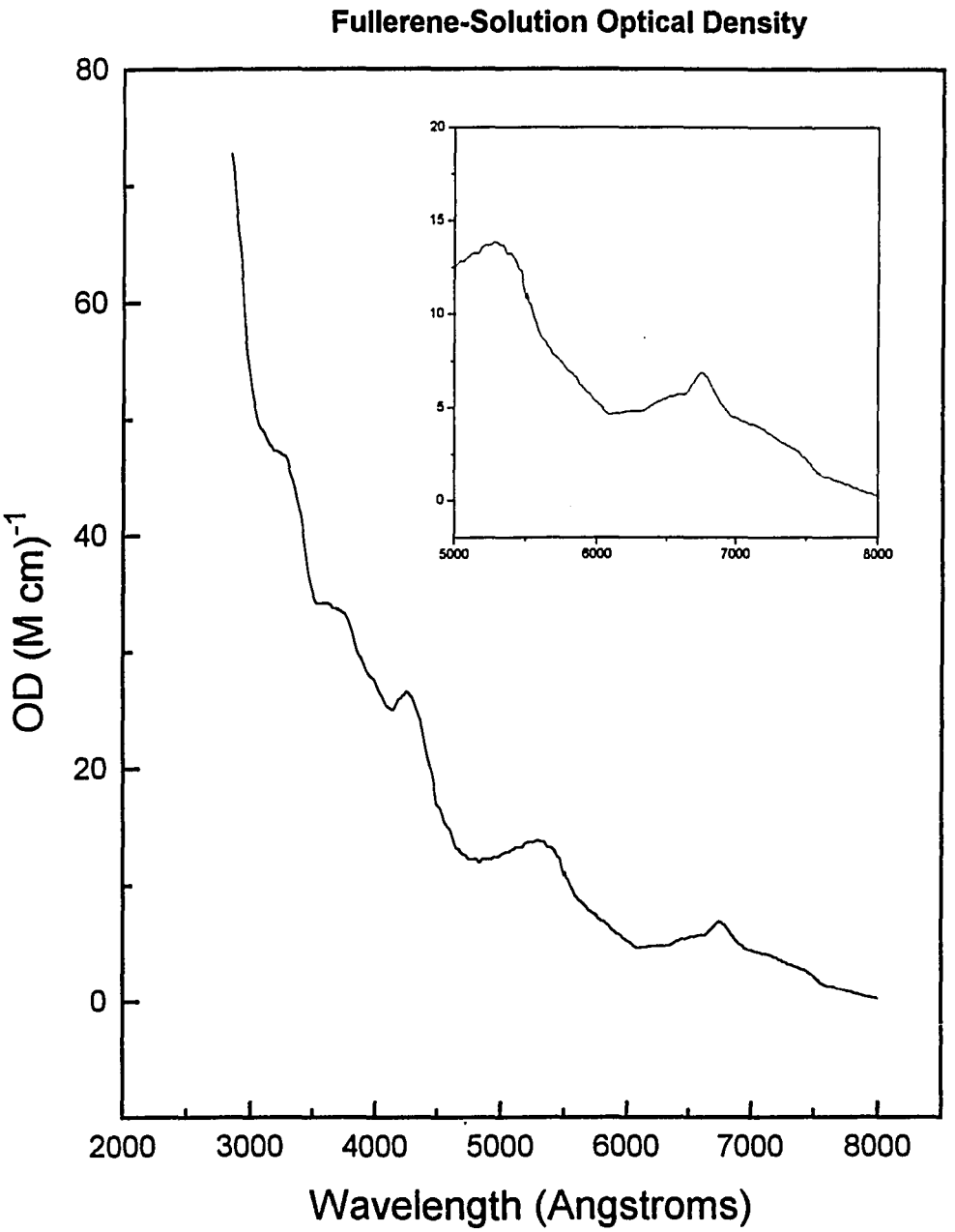

Figure A.41: Molar concentration-normalized C_{78} UV-Visible absorption spectrum from reference [35].

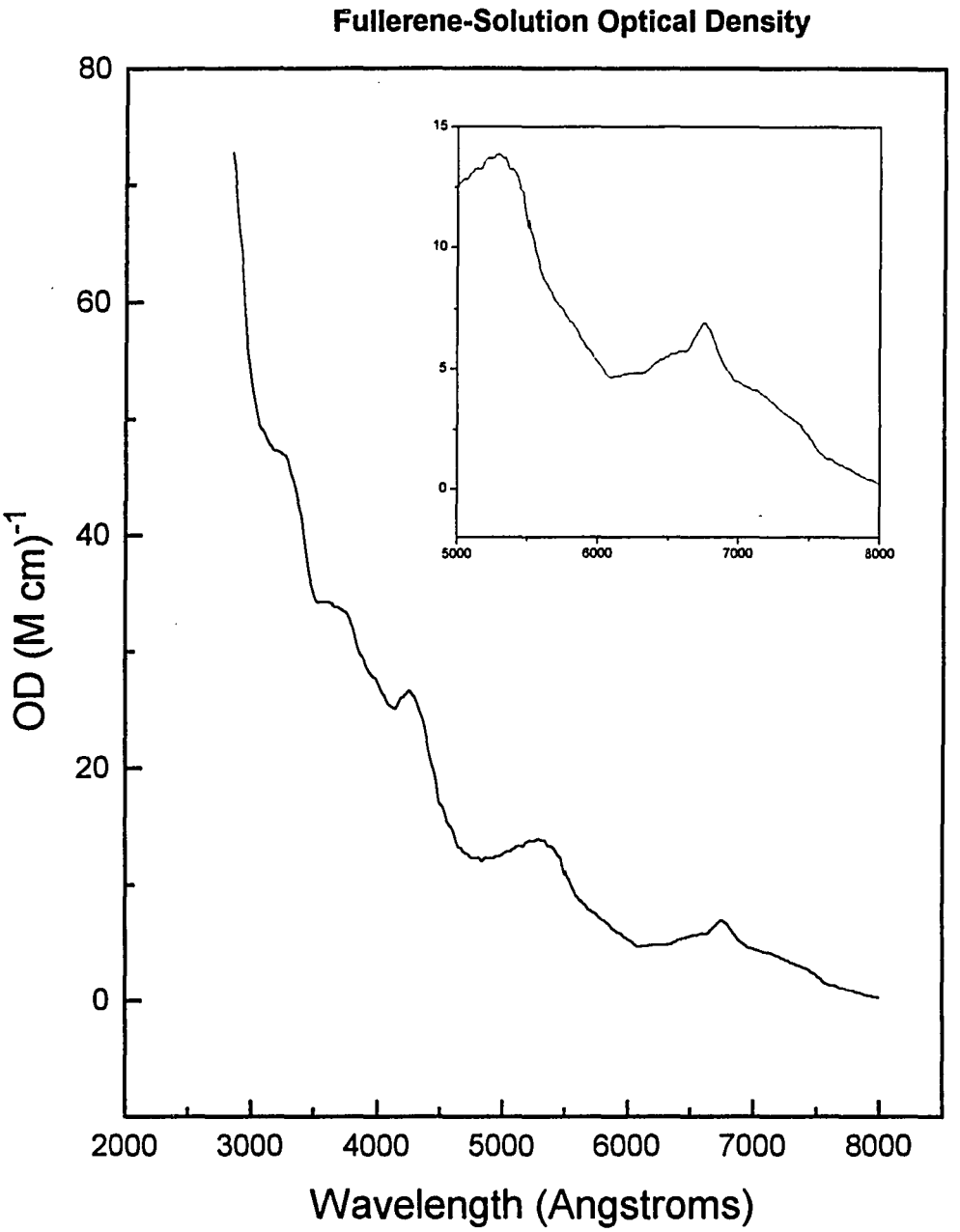

Figure A.42: Molar concentration-normalized C_{84} UV-Visible absorption spectrum from reference [36].

Note that the absolute values for C_{84} concentrations given by this analytical technique may be in error due to the ad-hoc normalization constant used. However, the slopes of the lines shown in Figs. 3.15-3.18 are independent of this absolute error.

REFERENCES

[1] E.A. Rohlfing, D.M. Cox, and A. Kaldor, *Production and Characterization of Supersonic Cluster Beams*, J. Chem. Phys. **81**, 3322-3330 (1984).

[2] H.W. Kroto, J.R. Heath, S.C. O'Brien, R.F. Curl, and R.E. Smalley C_{60}*: Buckminsterfullerene*, Nature Lond. **318**, 162-163 (1985).

[3] W. Krätschmer, L.D. Lamb, K. Fostiropoulos, and D.R. Huffman, *Solid C60: A New Form of Carbon*, Nature **347**, 354-358 (1990).

[4] J.B. Howard, A.L. Lafleur, Y. Makarovsky, S. Mitra, C.J. Pope, and T.K. Yadav, *Fullerene Synthesis in Combustion*, Carbon **30**(8), 1183-1201 (1992).

[5] R. Taylor, G.J. Langley, H.W. Kroto, and D.R.M. Walton, *Formation of* C_{60} *by Pyrolysis of Naphthalene*, Nature **366**, 728-731 (1993).

[6] M. Zumwalt, *The Role of Polycyclic Aromatic Hydrocarbons in the Study of Fullerene Formation*, Ph.D. Dissertation, University of Arizona (1995).

[7] P.R. Buseck, S.J. Tsipursky, and R.L. Hettich, *Fullerenes From the Geological Environment*, Science **257**, 215-217 (1992).

[8] T.K. Daly, P.R. Buseck, P. Williams, and C.F. Lewis, *Fullerenes from a Fulgurite*, Science **259**, 1599-1601 (1993).

[9] F.R. di Brozolo, T.E. Bunch, R.H. Fleming, and J. Macklin, *Fullerenes in an Impact Crater on the LDEF Spacecraft*, Nature **369**, 37-40 (1994).

[10] R.F. Bunshah, S.K. Jou, G.K.S. Prakash, H.J. Doerr, L. Issacs, A. Wehrsig, C. Yeretzian, H. Cynn, and F.N. Diederich, *Fullerene Formation in Sputtering and Electron-Beam Evaporation Processes*, J. Phys. Chem **96**, 6866

(1992).

[11] G. Peters and M. Jansen, *A New Fullerene Synthesis*, Angew. Chem. Int. Ed. Engl. **31**, 223 (1992).

[12] Y. Chai, T. Guo, C.M. Jin, R.E. Haufler, L.P.F. Chibante, J. Fure, Wang, J.M. Alford, and R.E. Smalley, *Fullerenes With Metals Inside*, J. Phys. Chem. **95**, 7564 (1991).

[13] R.E. Haufler, Y. Chai, L.P.F. Chibante, J.J. Conceicao, C.M. Jin, Wang, S. Maruyama, and R.E. Smalley, *Carbon Arc Generation of C_{60}*, Mater. Res. Soc. Proc. **206**, 627-638 (1991).

[14] L.D. Lamb, D.R. Huffman, *Fullerene Production*, J. Phys. Chem. Solids **54**(12), 1635-1643 (1993).

[15] D.H. Parker, P. Wurz, K. Chatterjee, K.R. Lykke, J.E. Hunt, M.J. Pellin, J.C. Hemminger, D.M. Gruen, and L.M. Stock, *High-Yield Synthesis, Separation, and Mass-Spectrometric Characterization of Fullerenes C60 to C266*, JACS **113**, 7499-7503 (1991).

[16] R.E. Haufler, Techniques of Fullerene Production. In *Proceedings of the Symposium on Recent Advances in the Chemistry and Physics of Fullerenes and Related Materials* (K.M. Kadish and R.E. Ruoff, eds.), (1994) The Electrochemical Society, Inc., NJ.

[17] Z. Slanina, J.M. Rudzinski, M. Togasi, and E. Osawa, *On Relative Stabililty Reasoning for Clusters of Different Dimensions: An Illustration with the C_{60}-C_{70} System*, Thermochim. Acta **140**, 87-95 (1989).

[18] T.G. Schmalz, W.A. Seitz, D.J. Klein, and G.E. Hite, *Elemental Carbon Cages*, J. Am. Chem. Soc. **110**, 1113-1127 (1988).

[19] J.R. Heath, Synthesis of C_{60} from Small Carbon Clusters: a Model Based on Experiment and Theory. In *Fullerenes: Synthesis, Properties, and Chemistry*

of Large Carbon Clusters (ACS Sympos. Ser., No. 481) (ed G.S. Hammond & V.J. Kuck), 1-23. Washington, D.C.: American Chemical Society.

[20] R.F. Curl, *On the Formation of Fullerenes*, Phil. Trans. R. Soc. Lond. A **343**, 19-32 (1993).

[21] A.W. Adamson, *A Textbook of Physical Chemistry*, Academic Press, New York, 60-69 (1973).

[22] F. Reif, *Fundamentals of Statistical and Thermal Physics*, McGraw-Hill Book Company, New York (1965).

[23] M.T. Bowers, P.R. Kemper, G. von Helden, and P.A.M. van Koppen, *Gas-Phase Chromatography: Transition Metal State Selection and Carbon Cluster Formation*, Science **260**, 1446-1451 (1993).

[24] G. von Helden, P.R. Kemper, N.G. Gotts, and M.T. Bowers, *Isomers of Small Carbon Cluster Anions: Linear Chains with up to 20 Atoms*, Science **259**, 1300-1302 (1993).

[25] H.D. Beckhaus, C. Ruchardt, M. Kao, F.N. Diederich, and C.S. Foote, *The Stability Of Buckminsterfullerene C_{60} - Experimental Determination Of The Heat Of Formation*, Angew. Chem. **31**, 63 (1992).

[26] C. Pan, M.P. Sampson, Y. Chai, R.H. Hauge, and J.L. Margrave, *Heats Of Sublimation from a Polycrystalline Mixture of C_{60} and C_{70}*, J. Phys. Chem **95**, 2944-2946 (1991).

[27] J. Tersoff, *Energies of Fullerenes*, Phys. Rev. B **46**(23), 15546-15548 (1992).

[28] B.L. Zhang, C.H. Xu, C.Z. Wang, C.T. Chan, and K.M. Ho, *Systematic Study Of Structures And Stabilities Of Fullerenes*, Phys. Rev. B **46**(11), 7333-7336 (1992).

[29] T.J. Lenosky, X. Gonze, M. Teter, and V. Elser, *Energetics of Negatively Curved Graphitic Carbon*, Nature **355**, 333-335 (1992).

[30] L.V. Gurvich, I.V. Veyts, C.B. Alcock, and V.S. Iorish (eds), *Thermodynamic Properties of Individual Substances*, Hemisphere Publishing Corporation, New York (1989).

[31] K. Raghavachari and J.S. Binkley, *Structure, Stability, and Fragmentation of Small Carbon Clusters*, J. Chem. Phys. **87**, 2191-2197 (1987).

[32] A.N. Pargellis, *Estimating Carbon Cluster Binding Energies from Measured C_n Distributions, $n \leq$ 10*, J. Chem. Phys. **93**(3), 2099-2108 (1990).

[33] X. Liu, T.G. Schmalz, and D.J. Klein, Reply to comment on *Favourable Structures for Higher Fullerenes*, Chem. Phys. Lett. **192**, 331-331 (1992).

[34] F.N. Diederich, R. Ettl, Y. Rubin, R.L. Whetten, R. Beck, M. Alvarez, S. Anz, D. Sensharma, F. Wudl, K.C. Khemani, and A. Koch, *The Higher Fullerenes: Isolation and Characterization of C_{76}, C_{84}, C_{90}, C_{94}, and $C_{70}O$, and Oxide of $D_{5h}-C_{70}$*, Science **252**, 548-551 (1991).

[35] F.N. Diederich, R.L. Whetten, C. Thilgen, R. Ettl, I. Chao, and M.M. Alvarez, *Fullerene Isomerism - Isolation of $C_{2v}-C_{78}$ and $D3-C_{78}$*, Science **254**, 1768-1770 (1991).

[36] R. Ettl, I. Chao, F.N. Diederich, and R.L. Whetten, *Isolation Of C76, A Chiral (D2) Allotrope Of Carbon*, Nature **353**, 149-153 (1991).

[37] W.H. Press, S.A. Teukolsky, W.T. Vetterling, and B.P. Flannery, *Numerical Recipes in C: The Art of Scientific Computing*, Cambridge University Press, Cambridge (1992).